OF RODENTS AND RANDOMNESS: MACROECOLOGICAL APPROACHES TO COMMUNITY STRUCTURE

By

RENATA M. DIAZ

A DISSERTATION PRESENTED TO THE GRADUATE SCHOOL
OF THE UNIVERSITY OF FLORIDA IN PARTIAL FULFILLMENT
OF THE REQUIREMENTS FOR THE DEGREE OF
DOCTOR OF PHILOSOPHY

UNIVERSITY OF FLORIDA

2022

To *R, K, r,* and *h*.

ACKNOWLEDGEMENTS

I will always be grateful to my dissertation advisor, Morgan Ernest, and my committee, Ethan White, Jamie Gillooly, and Justin Kitzes, for five years' of support and guidance as I have found my way through these projects. Throughout this journey, my mentors have consistently given me the encouragement and freedom to pursue challenging and adventurous projects, and modeled an approach to science grounded in curiosity, kindness, and bravery. I hope to bring a similar spirit to my future endeavors.

I am equally grateful to the ones who have shared this path with me over the years. In particular: Hao Ye, for being a steady and wise teacher on topics ranging from computational ecology, to cycling, to combinatorics; Ellen Bledsoe, for being a role model and a friend, from my very first weeks as a weecologist; Sam Zlotnik, for long walks and an appreciation for creatures; Pat Dumandan, for bringing joy and fresh perspective to the lab; and especially Jerald Pinson, for sharing stillness, wonder, and mirth.

Fundamentally, this dissertation is for my family. My mother, Katie, is a scientist in the purest way, and perpetually inspires me to find something new to explore in the natural world. My father, Ricardo, taught me that no matter how abstract or sophisticated a theory may seem, on some level it is about rats; and that sometimes a bicycle holds more answers than a supercomputer. My sister, Rosalind, brings wisdom and lightness to every challenge, and I am grateful every day that there are two of us. Finally, Hatter never forgets to remind me to love the little things in life, and gives me a reason to come home even on the darkest nights.

TABLE OF CONTENTS

LIST OF TABLES

LIST OF FIGURES

LIST OF OBJECTS

Objects page

LIST OF ABBREVIATIONS

AICc	Akaike information criterion adjusted for small sample sizes
ANOVA	Analysis of variance
BBS	North American Breeding Bird Survey
CB	*Chaetodipus baileyi*
CB_C	Total metabolic flux of *Chaetodipus baileyi* on control plots
CB_E	Total metabolic flux of *Chaetodipus baileyi* on exclosure plots
$Etot$	Total community-wide metabolic flux
$Etot_C$	Total community-wide metabolic flux on control plots
$Etot_E$	Total community-wide metabolic flux on exclosure plots
FIA	Forest Inventory and Analysis dataset
GLS	Generalized least squares
GLM	Generalized linear model
ISD	Individual size distribution
KR	Kangaroo rat (*Dipodomys spp.*)
KR_C	Total metabolic flux of kangaroo rats on control plots
KR_E	Total metabolic flux of kangaroo rats on exclosure plots
N	Total abundance
S	Species richness
SAD	Species abundance distribution
SG	Small granivore
SG_C	Total metabolic flux of small granivores on control plots
SG_E	Total metabolic flux of small granivores on exclosure plots

Abstract of Dissertation Presented to the Graduate School
of the University of Florida in Partial Fulfillment of the
Requirements for the Degree of Doctor of Philosophy

OF RODENTS AND RANDOMNESS: MACROECOLOGICAL APPROACHES TO COMMUNITY STRUCTURE

By

Renata M. Diaz

August 2022

Chair: S. K. Morgan Ernest
Major: Interdisciplinary Ecology

The system-wide attributes of ecological communities - such as community-level abundance, biomass, and metabolic flux, and how these are distributed among species and organisms - emerge from a web of shifting environmental constraints, diverse species interactions, and ubiquitous mathematical rules. While this apparent complexity can present a challenge to synthesis in community ecology, a macroecological perspective embraces ecological complexity as a path towards general understanding. In this dissertation, I use a telescoping macroecological perspective to explore how these factors shape community properties and determine how they change over time, building from a granular focus on species interactions in a well-studied experimental system, to successively broader spatial and conceptual scales in pursuit of general insights. In chapter 1 (the introduction), I offer an overview of the macroecological approach as it applies to community ecology and the specific vignettes in this dissertation. In chapter 2, I use a long-term experiment on desert rodents to disentangle how shifting environmental conditions and species interactions modulate the impact of species loss on community function. In chapter 3, I leverage modern computational approaches to show how changes in community structure modulate nuanced relationships between the long-term trends in size- and individuals- based currencies of community function. In chapter 4, I borrow tools and conceptual frameworks from statistical mechanics to explore what common ecological patterns stand to teach us about ecological, as opposed to statistical, processes. Finally, in chapter 5 (the conclusion), I offer

concluding reflections on the current landscape of prospects and challenges associated with a macroecological lens on community structure and function.

CHAPTER 1
INTRODUCTION

The interplay between system-specific natural history narratives and ubiquitous ecological or even mathematical rules that combine to determine how abundance, biomass, and resource use are distributed among species and organisms and across different levels of organization in ecological communities lies at the core of community ecology [61, 10]. A macroecological approach integrates classic modalities of ecological inquiry with conceptual frameworks drawn from across the scope of complex systems studies to disentangle phenomena specific to particular systems from general phenomena that reflect processes that operate across diverse taxonomic, geographic, and temporal contexts [8, 72]. In this dissertation, I adopt a macroecological perspective to understanding the structure and function of ecological communities, working from a narrow, system-specific focus on a well-studied long-term experiment, to a broad taxonomic and conceptual perspective on the interplay between combinatorics, statistical mechanics, and community ecology.

In chapter 2 [19], I use 30 years' of accumulated data and natural history knowledge to explore the effects of species loss on community function in an experimentally manipulated desert rodent community. Understanding how community function responds to species loss, and how the effects of species loss interact with shifting environmental conditions, is a key problem for biodiversity science in the current era of unprecedented ecological change. In this system, compensation due to functional redundancy temporarily buffered community function against species loss [26]. However, because similar, but non-identical, rodent species have responded differently to changes in environmental conditions over time, this compensatory effect has broken down, leaving community function highly sensitive to the loss of keystone species.

In chapter 3, I undertake a continental-scale comparison across communities to explore how shifts in community-wide body size modulate the long-term dynamics of individual abundance, biomass, and energy use in North American breeding birds. Although individual abundance and size and energy-based currencies are intrinsically linked, they capture different dimensions of community function, and shifts in community size structure can decouple the dynamics of different currencies [114, 49, 84]. I find that, in nearly one third of communities, changes in the

community size structure result in qualitatively different trajectories for biomass and total abundance over the past 30 years. As a result, while trends in individual abundance are dominated by declines, trends in total biomass are evenly split between declines and increases.

In chapter 4 [20], I step further back to examine how fundamental mathematical constraints inform our understanding of ecological ”laws”. Common patterns in community ecology, such as the ”hollow-curve” or J-shaped species abundance distribution (SAD), emerge from a combination of biological processes and ubiquitous mathematical constraints on the emergent properties of complex systems [80, 65]. Disentangling the signal of ecological processes from these mathematical constraints can provide new sources of inferential power linking pattern to process in community ecology [47]. I use combinatorics to characterize the mathematical constraint on the SAD, and compare the SADs of 22,000 empirically-observed communities to these ”statistical baselines”. This reveals that, while empirical SADs often match their statistical baselines, a substantial minority of real SADs deviate from these baselines - leaving an important role for ecological processes in shaping these distributions.

CHAPTER 2
MAINTENANCE OF COMMUNITY FUNCTION THROUGH COMPENSATION BREAKS DOWN OVER TIME IN A DESERT RODENT COMMUNITY

2.1 Background

Determining the extent to which community-level properties are affected by species loss, and how and why this changes over time, is key for understanding how communities are structured and how community function may respond to future perturbations [41]. When species are lost from a community, their contributions to community function (e.g. total productivity or resource use) are also directly lost. Community function may be maintained, however, if in the new community context, species that remain perform similar functions to the species that were lost, and compensate for the decline in function directly caused by species loss - i.e., functional redundancy [111, 110, 26, 94, 41]. When compensation via functional redundancy occurs among consumers with a common resource base, it is consistent with a zero-sum competitive dynamic, in which resources not used by one species are readily absorbed by competitors, and any increases in the abundance of one species must come at the direct expense of others [108, 27].

Because the response of system-level function to species loss is partially determined by the degree of functional redundancy in a community, processes that cause functional redundancy to change over time can have important consequences for the long-term maintenance of ecosystem function. Colonization events may buffer community function against species loss, if a community gains species that perform similar functions to the species that were lost [26, 62]. The ability of colonization to supply functionally redundant species depends on the species (and traits) present in the broader metacommunity, and on the rate of dispersal supplying appropriate species to local communities [62].

Even without the addition of new species and traits, however, functional redundancy within a consistent set of coexisting species may fluctuate over time. While, in theory, functional redundancy may occur via the special case of complete niche neutrality (e.g. [52]), it may also occur in niche-structured systems that contain species that share some traits but differ along other niche axes [104]. In these systems, if similar, but non-identical, species respond to environmental change in similar ways, functional overlap can be maintained or even strengthened. However, if

niche differences cause species to respond differently to changing conditions, the degree of functional overlap between those species may decline, resulting in a breakdown in compensation [66, 32]. Over time, as metacommunity dynamics and changing environmental conditions modulate functional redundancy within a community, the extent to which community function is robust to species loss - and the strength of zero-sum competition - may also be dynamic and context-dependent.

Despite logical conceptual support, and evidence from experimental microcosms [32], there is little empirical documentation of how, and through which mechanisms, temporal changes in functional redundancy modulate the effect of species loss on ecosystem function in natural assemblages. Although relatively plentiful, observational data cannot unambiguously detect compensation through functional redundancy, and even short-term experiments may not be sufficient to capture temporal variation in compensation [26, 51]. In contrast, long-term manipulative experiments are uniquely suited to address this question. In long-term experiments in which key species are removed from a community over an extended period of time, the impact of species loss on community function can be directly quantified by comparing community function between complete and manipulated assemblages. As metacommunity dynamics and environmental conditions shift over time, long-term monitoring can reveal how these processes contribute to changes in functional redundancy and ecosystem function across different time periods. Due to the financial and logistical resources required to maintain and monitor whole-community manipulations over long timescales, these experiments are rare in natural systems representative of realistic evolutionary, geographic, and environmental constraints [53].

Here, we use a 30-year experiment on desert rodents to investigate how shifts in functional redundancy alter the effect of species loss on community function over time. In this study, kangaroo rats (*Dipodomys* spp.), the largest and competitively dominant species in the rodent community, have been removed from a subset of experimental plots to explore how the loss of key species affects community function, measured as community-level metabolic flux ("total energy use", or *Etot*) or total biomass [29]. For systems of consumers with a shared resource

base, such as this community of granivorous rodents, *Etot* reflects the total amount of resources being processed by an assemblage, and total biomass directly reflects standing biomass. Both are important metrics of community function [60, 26]. Long-term monitoring of this experiment has documented repeated shifts in the habitat and species composition of this system, resulting in distinct time periods characterized by different habitat conditions and configurations of the rodent community [14]. Abrupt reorganization events in community composition occurred in 1997 and in 2010, associated with the establishment and subsequent decline of the pocket mouse *Chaetodipus baileyi*. *C. baileyi* is similar in size, and presumably other traits, to kangaroo rats, and its establishment in 1996-97 drove a pronounced increase in compensation due to functional redundancy between *C. baileyi* and kangaroo rats [26, 104]. Over the course of this experiment, shifting environmental conditions have caused the habitat at the study site to transition from desert grassland to scrub, driving a shift in baseline rodent community composition away from kangaroo rats and favoring other, smaller, granivores [7, 27]. By making comparisons across these time periods, we explored how shifts in community composition and functional overlap among the same species have contributed to long-term changes in the effect of species loss on community function.

2.2 Methods

2.2.1 The Portal Project

The Portal Project consists of a set of 24 fenced experimental plots located approximately 7 miles east of Portal, AZ, USA, on unceded land of the Chiricahua Apache. Beginning in 1977, kangaroo rats (*Dipodomys spectabilis*, *D. merriami*, and *D. ordii*) have been experimentally excluded from a subset of these plots (exclosures), while all other rodents are allowed access through small holes cut in the plot fencing. Control plots, with larger holes, are accessible to all rodents, including kangaroo rats. Rodents on all plots are censused via monthly bouts of live-trapping. Each individual captured is identified to species and weighed. For additional details on the site and methodology of the Portal Project, see [29].

2.2.2 Data

We used data for control and exclosure plots from February 1988 until January 2020. The experimental treatments for some plots have changed over time, and we used the subset of plots that have had the same treatments for the longest period of time [29]. Four control plots, and five exclosure plots, met these criteria. In order to achieve a balanced sample, we randomly selected four exclosure plots for analysis. We divided the timeseries into three time periods defined by major transitions in the rodent community surrounding the establishment and decline of *C. baileyi* [26, 14]. The first time period (February 1988-June 1997) precedes *C. baileyi*'s establishment at site. We defined *C. baileyi*'s establishment date as the first census period in which *C. baileyi* was captured on all exclosure plots (following [4]). During the second time period (July 1997-January 2010), *C. baileyi* was abundant on both exclosure and control plots. This time period ended with a reorganization event in which C. balieyi became scarce sitewide. We used January 2010, the midpoint of the 95% credible interval for the date of this reorganization event as estimated in [14], as the end date for this time period. The last time period spans from Feburary 2010-January 2020. For each individual rodent captured, we estimated the individual-level metabolic rate using the scaling relationship between individual body mass and metabolic rate $b = 5.69 * (m^{0.75})$, where m is body mass in grams and b is metabolic rate (for details, see [114]). We calculated treatment and species-level energy use as the sum of the appropriate individuals' metabolic rates, and total biomass as the sum of individuals' body mass measurements.

2.2.3 Statistical analysis of rodent community energy use and biomass

Here, we describe analyses for energy use. For biomass, we repeated these analyses substituting biomass values for energy use throughout. For all variables, we combined data for all plots within a treatment in each monthly census period and calculated treatment-level means. This is necessary to calculate compensation, and we treated other variables in the same way to maintain consistency. A provisional plot-level analysis yielded qualitatively equivalent results (Appendix A). To measure the overall impact of kangaroo rat removal on *Etot*, we calculated a "total energy ratio" as the ratio of treatment-level *Etot* for kangaroo-rat exclosure plots relative to

unmanipulated control plots, i.e. $Etot_E/Etot_C$ where $Etot_E$ and $Etot_C$ are total energy use on exclosures and controls, respectively [104, 4]. This ratio is distinct from compensation, which we defined as the proportion of the energy made available by kangaroo rat removal taken up via compensatory increases in energy use by small granivores (all granivores other than kangaroo rats; *Baiomys taylori*, *C. baileyi*, *Chaetodipus hispidus*, *Chaetodipus intermedius*, *Chaetodipus penicillatus*, *Perognathus flavus*, *Peromyscus eremicus*, *Peromyscus leucopus*, *Peromyscus maniculatus*, *Reithrodontomys fulvescens*, *Reithrodontomys megalotis*, and *Reithrodontomys montanus*). We calculated this as $(SG_E - SG_C)/KR_C$, where SG_E and SG_C are the amount of energy used by small granivores (SG) on exclosure and control plots, respectively, and KR_C is the amount of energy used by kangaroo rats (KR) on control plots [26]. To compare these variables across time periods, we used generalized least squares models (GLS; the R package *nlme* [86]) of the form $(SG_E - SG_C)/KR_C = timeperiod$, for compensation, and $Etot_E/Etot_C = timeperiod$, for the total energy ratio. We included a continuous-time autoregressive temporal autocorrelation term to account for temporal autocorrelation between values from monthly census periods within each multi-year time period (for details of model selection, see Appendix A). To evaluate change in baseline community composition over time, we calculated the proportion of treatment-level energy use accounted for by kangaroo rats on control plots in each census period ($KR_C/Etot_C$). Proportional energy use is bounded 0-1 and is therefore not appropriate for GLS, so we compared values across time periods using a binomial generalized linear model (GLM) of the form $KR_C/Etot_C = timeperiod$. Finally, we calculated the proportional energy use accounted for by *C. baileyi* (CB) on exclosure and control plots in each census period ($CB_E/Etot_E$ and $CB_C/Etot_C$, respectively). *C. baileyi* was not present at the site prior to 1996, and we restricted the analysis of *C. baileyi* proportional energy use to the second two time periods. We compared *C. baileyi* proportional energy use over time and across treatments using a binomial GLM of the form $CB_E/Etot_E = timeperiod + treatment$. For all models, we calculated estimated means and 95 confidence or credible intervals for time-period (and, for *C. baileyi*, treatment) level values, and contrasts between time periods (and, for *C. baileyi*, treatments), using the R package *emmeans*

[63]. Analyses were conducted in R 4.0.3 [92]. Data and code are archived at https://doi.org/10.5281/zenodo.5544361 and https://doi.org/10.5281/zenodo.5539880.

2.3 Results

The impact of kangaroo rat removal on community function has changed repeatedly over time, through a combination of abrupt shifts in compensation associated with *C. baileyi*, and long-term changes in baseline community composition sitewide (Figure 2-1). These dynamics are qualitatively identical whether function is measured as total energy use (Figure 2-1; Appendix A) or total biomass (Appendix A). The first shift coincided with *C. baileyi*'s establishment in the community beginning in 1996-97 (Figure 2-1D). *C. baileyi* rapidly became dominant on exclosure plots and dramatically increased compensation (Figure 2-1B). From 1997-2010, small granivores compensated for an average of 58% of kangaroo rat energy use on control plots (95% interval 48-67%), an increase from an average of 18% from 1988-1997 (95% interval 8-29%; contrast $p < 0.001$; for complete results of all models, see Appendix A) from 1997-2010. With *C. baileyi*'s addition to the community, the total energy ratio (on exclosures relative to controls; Figure 2-1A) increased from 30% (20-40%) to 71% (62-79%, contrast $p = 0.014$). In the second shift, beginning around 2010, *C. baileyi*'s abundance sitewide dropped precipitously (Figure 2-1D). *C. baileyi*'s proportional energy use dropped from an average of 72% (65-80%) to 26% (18-35%, contrast $p < 0.001$) on exclosure plots, and from 11% (6-16%) to essentially 0 on control plots (contrast $p < 0.001$). Other species of small granivore did not make compensatory gains to offset the decline in *C. baileyi* (Figure 2-1B). As a result, compensation declined from an average of 58% (48-67%) to 28% (17-38%, contrast $p = 0.002$), a level not significantly different from the 18% (8-29%, contrast $p = .44$) observed prior to *C. baileyi*'s establishment at the site. Somewhat paradoxically, while the total energy ratio also dropped following *C. baileyi*'s decline, from an average of 71% (62-79%) from 1997-2010 to 50% (40-60%, contrast $p = 0.0056$) from 2010-2020, it remained higher than its average of 30% (20-40%, contrast $p = 0.0144$) from 1988-1997 (Figure 2-1A). Over the course of the experiment, community composition shifted sitewide. In later years, kangaroo rats accounted for a lower proportion of baseline *Etot* than they

did at the beginning of the study (Figure 2-1C). From 1988-1997, kangaroo rats accounted for 92% (87-97%) of *Etot* on controls; after 1997, this dropped to an average of approximately 70% (1988-1997 compared to later time periods, both $p = .0004$; 1997-2010 and 2020-2020 not significantly different, $p = .976$). Because the proportion of *Etot* directly lost to kangaroo rat removal was smaller from 2010-2020 than from 1988-1997, the total energy ratio was higher from 2010-2020 than it was from 1988-1997 - even though there was not a detectable difference between the two time periods in the proportion of lost energy being offset through compensation.

2.4 Discussion

The dynamics of rodent community energy use at Portal illustrate that the role of functional redundancy in buffering community function against species loss fluctuates over time, due to changes in both species composition and in the degree of functional overlap among the same species. The 1997 increase in compensation, driven by *C. baileyi*'s establishment at the site, was a clear and compelling instance of colonization from the regional species pool overcoming limitations on functional redundancy [26, 62]. Although the small granivore species originally present in the community did not possess the traits necessary to compensate for kangaroo rats, *C. baileyi* supplied those traits and substantially, but incompletely, restored community function. In contrast, following the community reorganization event in 2010, *C. baileyi* remained present in the community, but ceased to operate as a partial functional replacement for kangaroo rats. This is consistent with fluctuating conditions modulating functional redundancy between similar, but non-identical, competitors. Kangaroo rats and *C. baileyi* are relatively similar in size and are demonstrably capable of using similar resources. However, *C. baileyi* prefers different, shrubbier microhabitats than kangaroo rats, and the two groups have been observed to replace each other in adjacent habitats [26]. We suggest that this study site, which has historically been dominated by kangaroo rats, constitutes marginal habitat for *C. baileyi*, and that, while conditions from 1997-2010 aligned sufficiently with *C. baileyi*'s requirements to create appreciable functional redundancy between kangaroo rats and *C. baileyi*, conditions since have caused this redundancy to break down. *C. baileyi*'s decline occurred immediately following a period of low plant

productivity and low rodent abundance community-wide, and in the decade following, the site experienced two long and severe droughts (Appendix A; [14]). These extreme conditions may themselves have limited *C. baileyi*'s fitness at the site, or the community-wide low abundance event may have temporarily overcome incumbency effects and triggered a community shift tracking longer-term habitat trends [103, 14]. Regardless of the proximate cause of *C. baileyi*'s decline, the fact that *C. baileyi* remains in the community, but no longer compensates for kangaroo rats, illustrates that changing conditions can have profound effects on community function by modulating the degree of functional redundancy within a consistent set of species.

While changes in compensation have contributed to changes in community function in this system, changes in compensation alone do not fully account for the long-term changes in the overall impact of kangaroo rat removal on *Etot*. Since 2010, although the ratio of *Etot* on exclosure plots relative to control plots declined coinciding with the breakdown in compensation associated with *C. baileyi*, it remained higher than the levels observed prior to 1997 (Figure 2-1A). This difference between the first and last time periods cannot be explained by an increase in compensation, as compensation from 2010-2020 was not greater than pre-1997 levels (Figure 2-1B). Rather, the increase in *Etot* on exclosure plots relative to control plots was the result of a long-term decrease in the contribution of kangaroo rats to *Etot* sitewide. Because kangaroo rats accounted for a smaller proportion of *Etot* on control plots from 2010-2020 than they did prior to 1997, their removal had a smaller impact on community function – even though there was not an increase in the degree to which small granivores compensated for their absence. In fact, the comparable levels of compensation achieved in the decades preceding and following *C. baileyi*'s dominance at the site suggest a relatively stable, and limited, degree of functional overlap between kangaroo rats and the original small granivores (i.e., excluding *C. baileyi*). Niche complementarity, combined with changing habitat conditions, may partially explain this phenomenon. It is well-documented that, while kangaroo rats readily forage in open microhabitats where predation risk can be relatively high, smaller granivores preferentially forage in sheltered microhabitats as an antipredator tactic [57]. Over the course of this experiment, the

habitat at this study site has transitioned from an arid grassland to a shrubland [7]. As sheltered microhabitats became more widespread, small granivores may have gained access to a larger proportion of resources and increased their share of *Etot* sitewide. However, kangaroo rats may have continued to use resources in open areas, which would have remained inaccessible to smaller granivores even on exclosure plots. The long-term reduction in the impact of kangaroo rat removal on community function, driven by niche complementarity and consistent niche partitioning, contrasts with the temporary compensatory dynamic driven by functional redundancy with *C. baileyi*. Although changes in the overall effect of species loss are sometimes treated interchangeably with compensation (e.g. [26] compared to [104]), it is important to recognize that multiple distinct pathways modulate the long-term impacts of species loss on community function. Particularly in strongly niche-structured systems, complementarity effects and fluctuations in functional redundancy may occur simultaneously, with complex and counterintuitive impacts on community function.

Overall, the decadal-scale changes in energy use among the Portal rodents underscore the importance of long-term metacommunity dynamics to the maintenance of community function following species loss (see [62]). Although a single colonization event may allow for temporary compensation via functional redundancy, as conditions shift, species that once compensated may no longer perform that function (see also [54]). Particularly if limiting similarity prevents similar competitors from specializing on precisely the same habitats [94], temporary, context-dependent compensation may be common. To maintain compensation over time, multiple colonization events, supplying species that are functionally redundant under different conditions, may be required. Depending on dispersal rates, and the diversity and composition of regional species pools, this may be unlikely or even impossible. At Portal, dispersal limitation introduced a 20-year delay in the compensatory response driven by *C. baileyi*. Theoretically, a new species capable of compensating for kangaroo rats, and better-suited to conditions at the site since 2010, could restore compensation under present conditions – but it is unclear whether this species exists or if it can disperse to this site. As ecosystems globally undergo reductions in habitat connectivity

and regional beta diversity, and enter novel climatic spaces, maintenance of community function via functional redundancy may grow increasingly rare and fragile [22, 117].

Finally, the long-term variability in functional redundancy documented here adds important nuance to our understanding of how zero-sum dynamics operate in natural assemblages. Theories invoking zero-sum dynamics, and tests for compensatory dynamics in empirical data, often treat a zero-sum dynamic as a strong and temporally consistent constraint [52, 51]. In this framing, any resources made available via species loss should immediately be taken up by other species. This is not consistent with the dynamics that occur at Portal, which has seen extended periods of time when resources are available on exclosure plots but are not used. Rather, these results are more consistent with a zero-sum constraint operating at metacommunity or evolutionary scales [108, 102, 62]. Over short timescales, or within a closed local assemblage, niche differences may weaken zero-sum effects, especially under fluctuating conditions. However, over larger temporal and spatial scales, dispersal or evolution may supply new species equipped to use available resources - via either functional redundancy, or niche complementarity allowing them to exploit novel niches. A long-term, metacommunity, and even macroevolutionary approach may be necessary to fully understand how zero-sum constraints, functional redundancy, and niche complementarity contribute to the maintenance of community-level function in the face of species extinctions and changing conditions over time.

2.5 Figures for Chapter 2

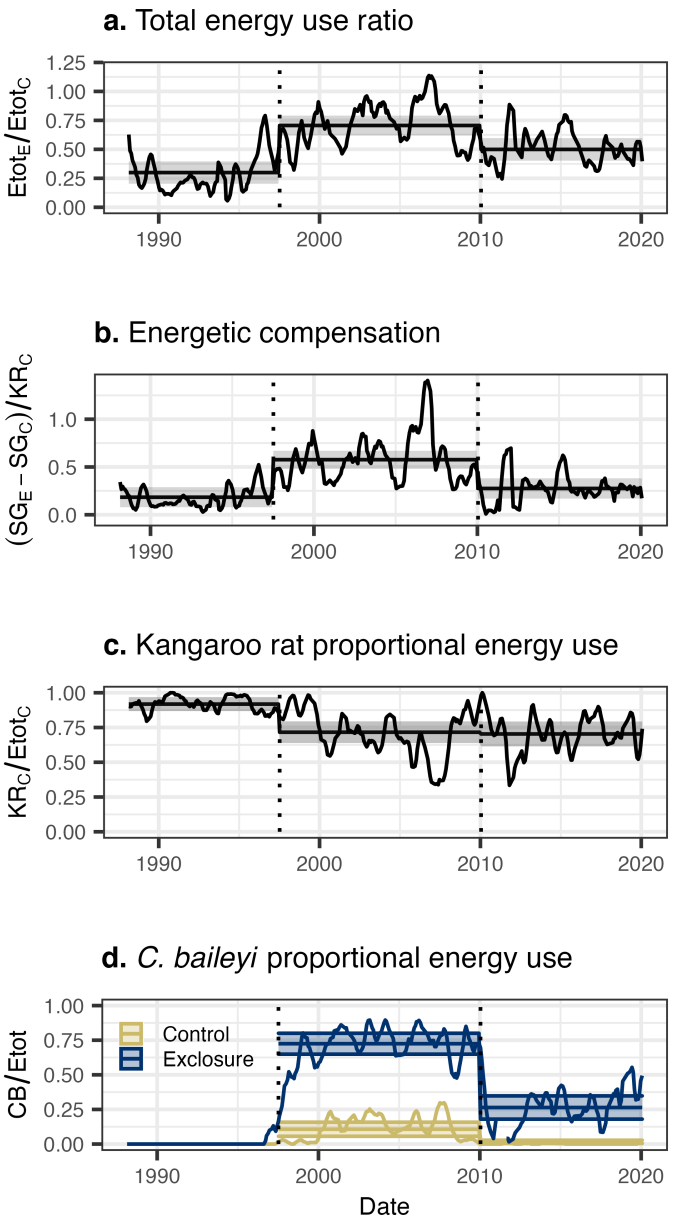

Figure 2-1. Dynamics of energy use and rodent community composition over time. Lines represent the ratio of total energy use on exclosure plots to control plots (a), 6-month moving averages of energetic compensation (b), and the share of community energy use accounted for by kangaroo rats on control plots (c), and by *C. baileyi* (d), on control (gold) and exclosure (blue) plots. Dotted vertical lines mark the boundaries between time periods used for statistical analysis. Horizontal lines are time-period estimates from generalized least squares (a, b) and generalized linear (c, d) models, and the semitransparent envelopes mark the 95% confidence or credible intervals.

CHAPTER 3
TEMPORAL CHANGES IN THE INDIVIDUAL SIZE DISTRIBUTION DECOUPLE LONG-TERM TRENDS IN ABUNDANCE, BIOMASS, AND ENERGY USE OF NORTH AMERICAN BREEDING BIRD COMMUNITIES

3.1 Background

Understanding the interrelated dynamics of size- and individuals-based dimensions of biological abundance is key to understanding trends in biodiversity in the Anthropocene. Total individual abundance - i.e. the total number of individual organisms present in a system - and size-based currencies, such as the total biomass or total metabolic flux ("energy use") of a system, are intertwined, but nonequivalent, measures of biological function. Abundance is most closely tied to species-level population dynamics, while size-based metrics more directly reflect assemblage-level resource use and contributions to materials fluxes at the broader ecosystem scale [77, 23, 16, 115]. While these currencies are naturally linked [77, 48], changes in size composition can decouple the dynamics of one currency from another [28, 23, 114, 115, 121]. This can mean that intuition from one currency may be misleading about others; a trend in numerical abundance might mask contrasting dynamics occurring with respect to biomass or total energy use [114]. Changes in size composition strong enough to decouple currencies may be symptomatic of important changes in ecosystem status - e.g. abundance-biomass comparison curves in the aquatic realm [84] or size-biased extinctions [123, 100]. In the Anthropocene, as ecosystems globally undergo unprecedented levels of ecological and functional change [33], it is especially important to understand long-term trends in individual abundance, total biomass, total energy use, and the relationship between these currencies.

At the community scale, changes in the relationship between size and abundance can signal important shifts in community structure and functional composition. To the extent that size is a proxy for other functional traits, changes or consistency in the community-level size structure (individual size distribution, ISD) over time may reflect processes related to niche structure [115, 84]. Strong size shifts can decouple the relationship between abundance and biomass. This is especially well-established in aquatic systems, where such changes in the scaling between abundance and biomass often signal ecosystem degradation [112, 59, 84]. Compensatory shifts in the size structure can buffer community function (in terms of biomass or energy use) against

changes in abundance [28, 114, 102]. Or, consistency in the size structure may maintain the relationship between size- and -abundance based currencies, even as species composition, total abundance, and total biomass and total energy use fluctuate over time, which can reflect consistency in the niche structure over time [50]. In contrast to terrestrial trees and aquatic systems, which have received considerable attention in this regard [59, 115], the relationships between community structure, total biomass, and individual abundance remain relatively unknown for terrestrial animals (but see [114]). Terrestrial animal communities exhibit size structure [106, 25], and case studies have demonstrated that size shifts can decouple the dynamics of individual abundance, biomass, and energy use for terrestrial animals [114, 121], but do not always do so [49]. Establishing generalities in these dynamics is especially pertinent in the Anthropocene, as these communities are experiencing extensive and potentially size-structured change, with implications at community, ecosystem, and global scales [123, 97].

Macroecological-scale synthesis on the interrelated dynamics of the ISD, total abundance, and community function for terrestrial animals has been constrained by 1) a lack of community-level size and abundance timeseries data for these systems [106, 115], and 2) appropriate statistical methods for relating change in the size structure to changes in abundance and function [106, 121]. In contrast to aquatic and forest systems, most long-term surveys of animal communities do not collect data on individuals' sizes across a full community (with the exception of small mammal studies, which have made major contributions to our understanding of the dynamics of size, abundance, and function for these systems; [114, 25, 49, 58]. Global, continental, or population-wide studies capture different phenomena [115, 73]. The ISDs for terrestrial animals, and specifically for determinate growing taxa (e.g. mammals, birds), are often complex, multimodal distributions strongly determined by community species composition [50, 106, 25, 121] and less statistically tractable than the power-law ISDs found in aquatic and tree systems [59, 115]. Quantifying change in the size structure, and relating this to change in community-wide abundance and function, is not as straightforward as computing and comparing slopes. As a result, we do not have a general understanding of either 1) how the size structures for

these systems behave over time or 2) the extent to which changes in community size structure decouple the community-level dynamics of abundance, biomass, and energy use in these systems.

Here, we begin to address this gap by exploring how temporal changes in the size structure modulate the relationship between total abundance, energy, and biomass for communities of North American breeding birds. We used allometric scaling to estimate community size and abundance data for the North American Breeding Bird Survey, and evaluated how changes in total abundance, biomass, and energy use have co-varied from 1988-2018. Specifically, we examined: 1) How often do these currencies change together vs. have decoupled dynamics?; 2) What are the dominant directions and magnitudes of the overall change over time and degree of decoupling between the currencies?; 3) To what extent do changes in species composition and community size structure translate into decoupling in the temporal trends of different currencies at the community scale?

3.2 Methods

Code to replicate these analyses is available online at https://github.com/diazrenata/diss-BBSsize and https://github.com/diazrenata/bbs-size-shifts.

3.2.1 Bird abundance data

We used data from the Breeding Bird Survey [83] to evaluate trends in abundance, biomass, and energy use. The Breeding Bird Survey consists of roughly 40 kilometer-long survey routes distributed throughout the United States and Canada. Routes are surveyed annually during the breeding season (predominately May-June), via 50 3-minute point counts during which all birds seen or heard are identified to species [83]. Sampling began in 1966, and routes have been added over time to a current total of roughly 3000 routes [83]). We take the route to be the "community" scale [106]. We filtered the Breeding Bird Survey data to remove taxa that are poorly sampled through the point-count methods used in the Breeding Bird Survey, following [44]. We accessed the data, and performed this preliminary cleaning and filtering, using the R package *MATSS* [120].

We explored trends in abundance, biomass, and energy use over the 30-year time period from 1988-2018. We selected these years to provide a temporal window sufficient to detect

long-term trends [17]), while allowing for a substantial number of routes. To avoid irregularities caused by missing time steps, we restricted the main analysis to routes that had been sampled in at least 27 of 31 years in this window ($n = 739$), and compared these results to a more strict selection of routes that were sampled in every year ($n = 199$). Results for this more conservative subset of routes were qualitatively the same as for the more inclusive selection of routes (Appendix B).

3.2.2 Estimated size data

The Breeding Bird Survey contains abundances for all species along a route in each year, but does not include measurements of individual body size. We generated body size estimates for individual birds assuming that intraspecific size distributions are normally distributed around a species' mean body size (following [106]). Using records of species' mean and standard deviation body sizes from [24], we drew individuals' body sizes from the appropriate normal distributions. For species for which there was not a standard deviation recorded in [24] (185 species affected, of 421 total), we estimated the standard deviation using an allometric scaling relationship between mean and standard deviation in body mass based on the records for which the standard deviation was provided. Using these records, we fit a linear model of the form $\log(\text{var}(m)) = \log(\bar{m})$), where m is body mass (model $R^2 = .89$), which yielded the scaling relationship $\text{var}(m) = 0.0047\bar{m}^{2.01}$ (see also [106] for this scaling relationship calculated on a slightly different subset of the Breeding Bird Survey). For species with multiple records in [24], we used the mean $\bar{m}$ and standard deviation of m across all records (averaging across sexes, subspecies, and records from different locations). We performed this averaging after estimating any missing standard deviation measurements.

We simulated individual-level body mass measurements for each individual bird observed by drawing from the normal distribution with the mean and standard deviation of body mass estimated for each bird's species [106]. For each individual bird, we estimated metabolic rate as $10.5(m^{0.713})$ [37, 78, 75]. For each route in each year, we computed total energy use, total biomass, and total abundance by summing over all individuals observed on that route in that year. This method does not incorporate intraspecific variation in body size across geographies or

changes in species' mean body size over time [24, 38]. However, it makes it possible to conduct macroecological studies of avian size distributions at a spatial and temporal scale that would otherwise be impossible [106]. An R package containing code to generate these size estimates is available at https://github.com/diazrenata/diss-BBSsize.

3.2.3 Comparing abundance- and size- based currencies

Comparing trends across different currencies is a nontrivial statistical problem. Because different currencies vary widely in their units of measure (e.g. abundance in the hundreds of individuals; total biomass in the thousands of grams), it is challenging to interpret differences in magnitude of slope across different currencies. Transformation and scaling using common approaches (such as a square-root transformation, or rescaling each currency to a mean of 0 and a standard deviation of 1) destroys information about the degree of variability within each currency that is necessary in order to make comparisons between currencies for the same timeseries.

Rather than attempting to compare slopes across currencies or to transform different currencies to a common scale, we used a simple null model to compare the observed dynamics for biomass and energy use to the dynamics that would occur in a scenario in which the species composition (and therefore, in this context, size structure) of the community was consistent throughout the timeseries, but in which total individual abundance varied over time consistent with the observed dynamics. For each route, we characterized the "observed" timeseries of total biomass and total energy use by simulating size measurements for all individuals observed in each time step and summing across individuals, using the method described above. We then simulated timeseries for "individuals-driven" dynamics of biomass and energy use incorporating observed changes in community-wide individual abundance over time, but under a scenario of consistent species (and therefore approximate size) composition over time. For each community, we characterized the timeseries-wide probability of an individual drawn at random from the community belonging to a particular species ($P(s_i)$) as each species' mean relative abundance taken across all timesteps:

$$P(s_i) = \frac{\Sigma_t^T \frac{n_{i,t}}{N_T}}{T}$$

where $n_{i,t}$ is the abundance of species i in timestep t, N_t is the total abundance of all species in timestep t, and T is the total number of timesteps. For each timestep t, we randomly assigned species' identities to the total number of individuals (of all species) observed in that time step (N_t) by drawing with replacement from a multinomial distribution with probabilities weighted according to $P(s)$ for all species. We then simulated body size measurements for individuals, and calculated total energy use and total biomass, following the same procedure as for the observed community. This characterizes the dynamics for size-based currencies expected if the species (and size) composition of the community did not change over time, but incorporating observed fluctuations in total individual abundance. We refer to these dynamics as "individuals-driven" dynamics.

3.2.4 Long-term trends

For each route, we evaluated the 30-year trend in biomass (or energy use) and compared this to the trend derived from the "individuals-driven" null model using generalized linear models with a Gamma family and log link (appropriate for strictly-positive response variables such as biomass or total energy use). We selected between four model formulas, corresponding to qualitatively different "syndromes" of change, to characterize 1) the trend in biomass (or energy use) over time and 2) whether this trend deviates from the trend expected given only changes in individual abundance:

- *biomass = year * dynamics* or *energy use = year * dynamics* in which "dynamics" refers to being either the "observed" or "individuals-driven" (null model) dynamics. This model fits a slope and intercept for the observed trend in biomass or energy use over time, and a separate slope and intercept for the trend drawn from the individuals-driven dynamics. We refer to this model as describing a syndrome of "Decoupled trends" between individuals-driven and observed dynamics.

- *biomass = year + dynamics* or *energy use = year + dynamics*. This model fits a separate intercept, but not slope, for the individuals-driven and observed dynamics. This model was never selected as the best-performing description of community dynamics.

- *biomass = year* or *energy use = year*. This model fits a temporal trend, but does not fit

separate trends for the observed and individuals-driven dynamics. We refer to this syndrome as "Coupled trends" between individuals-driven and observed dynamics.

- *biomass = 1* or *energy use = 1*. The intercept-only model describes no directional change over time for either the observed or individuals-driven dynamics, and we refer to this syndrome as describing "No directional change" for either type of dynamics.

We selected the best-fitting model for each route using AICc. In instances where multiple models had AICc scores within two AICc units of the best-fitting model, we selected the simplest model within two AICc units of the best score. We used the model predictions from each route's best-fitting model to characterize the direction and slope of each route's long term trends for individuals-driven (null) and biomass- or energy use-driven (observed) dynamics. For each route's best-fitting model, we extracted the predicted values for the first (usually 1988) and last (usually 2018) year sampled, for both the observed and null trajectories. We calculated the magnitude of change over time as the ratio of the last (2018) to the first (1988) value, and characterized the direction of the long-term trend as increasing if this ratio was greater than one, and decreasing if it was less than one.

3.2.5 Relating change in community structure to decoupling between individual- and size-based dynamics

We used dissimilarity metrics to explore the extent to which change in community structure propagates to decoupling between long-term trends in individual abundance and total biomass and energy use. These dissimilarity metrics are most readily interpretable when making pairwise comparisons (as opposed to repeated comparisons over a timeseries). We therefore made comparisons between the first and last five-year intervals in each timeseries, resulting in a "begin" and "end" comparison separated by a relatively consistent window of time across routes (usually 19-20 years). The use of five-year periods corrects for sampling effects [113]), smooths out interannual variability, and, by including a relatively large proportion $\frac{1}{3}$ of the total timeseries, partially mitigates the impact of scenarios where the start and end values do not align with the long-term trend.

We calculated three metrics to explore how changes in community composition and size structure translate into decoupling between individuals-driven and observed dynamics for biomass and energy use. First, we evaluated the change in average community-wide body size, calculated as the absolute log ratio of mean body size in the last five years relative to the mean body size in the first five years: absolute log ratio $= \ln \frac{\bar{m}_{last5}}{\bar{m}_{first5}}$ where $\bar{m}_{first5}$ and $\bar{m}_{last5}$ is the mean body size of all individuals observed in the first and last 5 years, respectively. We used the absolute log ratio in order to focus on the magnitude, rather than the direction, of change in body size (see also [101] for the use of the absolute log ratio to examine the magnitudes of differences between values). Large changes in community-wide average body size are, by mathematical necessity, expected to translate into decoupling between observed and abundance-driven dynamics.

Second, we calculated measures of turnover in the size structure and in species composition. We calculated turnover in the ISD using a measure inspired by an overlap measure that has previously been applied to species body size distributions in mammalian communities [93]. We characterized each "begin" or "end" ISD as a smooth probability density function by fitting a Gaussian mixture model (with up to 15 Gaussians, fit following [106]) to the raw distribution of body masses, and extracting the fitted probability density at 1000 evaluation points corresponding to body masses encompassing and extending beyond the range of body masses present in this dataset (specifically, from 0 to 15 kilograms; mean body masses in this dataset range from 2.65 grams, for the Calliope hummingbird *Selasphorus calliope*, to 8.45 kg, for the California condor *Gymnogyps californianus*). We rescaled each density function such that the total probability density summed to 1. To calculate the degree of turnover between two ISDs, we calculated the area of overlap between the two density smooths as
ISD turnover $= \sum \min(density1_i, density2_i)$ where $density1_i$ is the probability density from the density smooth for the first ISD at evaluation point i, and $density2_i$ is the probability density from the density smooth for the second ISD at that evaluation point. We subtracted this quantity from 1 to obtain a measure of turnover between two ISDs.

To evaluate turnover in species composition between the five-year time periods, we

calculated Bray-Curtis dissimilarity between the two communities using the R package *vegan* [86].

We tested whether routes whose dynamics were best-described by each "syndrome" of change – i.e. "Decoupled trends", "Coupled trends", or "No directional change" – differed in 1) the magnitude of change in mean body size; 2) turnover in the ISD over time; or 3) species compositional turnover (Bray-Curtis dissimilarity) over time. For change in mean body size, we fit an ordinary linear model of the form *absolute log ratio* = *syndrome*. We compared this model to an intercept-only null model of the *absolute log ratio* = *1*. Because our metrics for turnover in the ISD and species composition are bounded from 0-1, we analyzed these metrics using binomial generalized linear models of the form *ISD turnover* = *syndrome* and *Bray Curtis dissimilarity* = *syndrome*, and again compared these models to intercept-only null models. In instances where the model fit with a term for syndrome outperformed the intercept-only model, we calculated model estimates and contrasts using the R package *emmeans* [63].

3.3 Results

Of the 739 routes in this analysis, approximately 70% (500/739 for biomass, and 509/739 for energy use) exhibited syndromes of "Decoupled trends" or "Coupled trends" (that is, were best-described using a model incorporating a temporal trend in individuals-driven and/or biomass or energy use-driven dynamics (Table 3-1)). All results were qualitatively the same using a subset of 199 routes with complete temporal sampling over time (Appendix B). Trends driven by individual abundance, as reflected by the dynamics of a simple null model, were strongly dominated by declines (335 decreases and 165 increases for individuals-driven dynamics in biomass, and 355 decreases and 154 increases for individuals-driven dynamics in energy use; Figure 3-2; Table 3-2). However, for biomass, the long-term temporal trends were evenly balanced between increases and decreases (256 decreasing trends, and 244 increasing trends; Figure 3-2; Table 3-2). For energy use, there was a greater representation of decreasing trends than for biomass, but still less so than for strictly abundance-driven dynamics (329 decreasing trends and 180 increasing trends; Figure 3-2; Table 3-2).

These divergent aggregate outcomes in individual abundance, energy use, and especially biomass occurred due to decoupling in the long-term trends for these different currencies. For a substantial minority of routes (20% of all routes for biomass, and 7% of all routes for energy use), long-term dynamics were best-described as a syndrome of "Decoupled trends" (that is, with a different slope for biomass or energy use-driven dynamics than for the "null", individuals-driven, trend) (Table 3-1). When this decoupling occurred, it was dominated by instances in which the slope for individuals-driven dynamics was more negative than that for biomass or energy use (Figure 3-3).

Decoupling between the long-term trajectories of individual abundance and energy use or biomass is, by definition, indicative of some degree of change in the community size structure over time. Routes whose dynamics for biomass were best-described as syndromes of decoupled trends over time had a higher absolute log ratio of mean mass (i.e. greater magnitude of change, either increasing or decreasing, in mean mass over time) than routes with coupled or no directional trends (Figure 3-4; Appendix B). However, there was not a detectable difference in the degree of temporal turnover in the ISD overall (Figure 3-4; Appendix B), or in species composition (Figure 3-4; Appendix B), compared between routes that exhibited different syndromes of change.

3.4 Discussion

3.4.1 Abundance, biomass, and energy use are nonequivalent currencies

Simultaneously examining multiple currencies of community-level abundance revealed qualitatively different continent-wide patterns in the long-term trends for the number of individuals, total biomass, and energy use. While long-term trends in individual abundance were dominated by decreases, long-term trends in biomass were evenly split between increases and decreases, and trends in energy use were again dominated by declines (Figure 3-2). These different currencies, though intrinsically linked, describe nonequivalent dimensions of community function and reflect different classes of structuring processes [77]. Individual abundance is most directly linked to species-level population dynamics of the type often considered in classic,

particularly theoretical, approaches to studying competition, compensation, and coexistence (e.g. [52, 12]). Biomass most directly reflects the productivity of a community and its potential contributions to materials fluxes in the broader ecosystem context, whereas energy use - by taking into account the metabolic inefficiencies of organisms of different body size - characterizes the total resource use of a community and may come the closest to capturing signals of bottom-up constraints, "Red Queen" effects, or zero-sum competitive dynamics [108, 27, 28, 77, 114]. Our results underscore that, while trends in individual abundance, biomass, and energy use naturally co-vary to some extent, shifts in the community size structure can and do produce qualitatively different trends for these different currencies. These may reflect contrasting long-term changes in different types of community processes - for example, shifts in habitat structure that affect the optimal body sizes for organisms in a system, but do not result in overall changes in resource availability (e.g. [114]). Moreover, extrapolating the long-term trend from one currency to another may mask underlying changes in the community that complicate these dynamics. To appropriately monitor different dimensions of biodiversity change, it is therefore important to focus on the specific currency most closely aligned with the types of processes and dynamics - e.g. population fluctuations, resource limitation, or materials fluxes - of interest in a particular context.

3.4.2 For North American breeding birds, biomass has declined less than abundance or energy use

For communities with a decoupling in the long-term trends of biomass, energy use, and abundance, this decoupling is indicative of a directional shift in the size structure of the community. For the communities of breeding birds across North America considered here, the long-term trends in total biomass are often less negative than trends in total individual abundance or total energy use (Figure 3). This consistent (but not ubiquitous) signal corresponds to community-level increases in average body size that partially or completely buffer changes in total biomass against declines in the overall number of individuals. This contrasts with taxonomically general, global concerns that larger-bodied species are more vulnerable to extinction and population declines than smaller ones [123, 21, 100]. However, it is consistent with

previous findings from the Breeding Bird Survey [96]. The long-term trends for communities of different taxonomic groups, geographies, or temporal spans may show different effects related to different facets of global change and biodiversity responses. We also note that these increases in body size do not generally appear great enough to decouple the long-term trends in energy use from total individual abundance (Figure 3-3). Energy use scales nonlinearly with body size with an exponent less than 1, which means that community-wide increases in mean body size result in smaller increases in total energy use than in total biomass.

3.4.3 Complex relationships between compositional change and community-level properties

The decoupling between the long-term trends for biomass, individual abundance, and energy use demonstrated in many of the communities studied here is symptomatic of a directional shift in the size structure - in these instances, generally favoring larger bodied species. However, examining the community-wide dynamics of turnover in species composition and the overall size structure reveals that the relationship between changes in community structure and changes in the scaling between different currencies of community-wide abundance is considerably more nuanced than simple directional shifts in mean size. Routes that exhibit a statistically detectable decoupling between total biomass and total abundance show large changes in average body size compared to routes for which biomass and abundance either change more nearly in concert with each other or do not show temporal trends (Figure 3-4; Appendix B). This aligns naturally with mathematical intuition given the intrinsic relationship between average body size, total abundance, and total biomass. However, these routes are not extraordinary in terms of their overall degree of temporal turnover in either the size structure or in species composition. Rather, the levels of turnover in overall community size structure and species composition are comparable between routes that show decoupling between abundance and biomass, statistically indistinguishable trends, or no temporal trends in either currency (Figure 3-4; Appendix B).

For many communities, therefore, there has been appreciable change in species and size composition that does not manifest in a shift in the overall community-wide mean body size or

mean metabolic rate sufficient to decouple the dynamics of biomass, abundance, and energy use. These changes may signal changes in functional composition equally important as the ones that manifest in directional shifts in community-wide average body size. For the complex, multimodal size distributions that are the norm for avian communities [106], changes in the number and position of modes may be as important as changes in higher-level statistical moments such as the overall mean. At present, the field lacks the statistical tools and conceptual frameworks to quantify and interpret these nuanced changes, especially at the macroecological scale of the current study [106, 121]. However, this is an excellent opportunity for more system-specific work, informed by natural history knowledge and process-driven expectation, to characterize more nuanced changes in the size structure of specific communities and identify the underlying drivers of these changes. To facilitate these efforts in the context of the Breeding Bird Survey, the R package we have developed to characterize the individual size distributions for avian communities based on species' identities and/or mean body sizes is freely available for re-use and wider applications (https://github.com/diazrenata/diss-BBSsize; the general-use version of this package is currently in development at https://github.com/diazrenata/birdsize).

3.4.4 Summary and paths forward

This analysis demonstrates the current power, and limitations, of a data-driven macroecological perspective on the interrelated dynamics of community size structure and different dimensions of community-wide abundance for terrestrial animal communities. For breeding bird communities across North America, we find that changes in species and size composition produce qualitatively different aggregate patterns in the long-term trends of abundance, biomass, and energy use, highlighting the nuanced relationship between these related, but decidedly nonequivalent, currencies and reflecting widespread changes in community size structure that may signal substantive changes in functional composition. Simultaneously, the complex relationship between turnover in community species and size composition, and the scaling between different currencies of community-level abundance, highlights opportunities for synergies between recent computational and statistical advances, case studies grounded in

empiricism and natural history, and future macroecological-scale synthesis to realize the full potential of this conceptual space.

3.5 Figures for Chapter 3

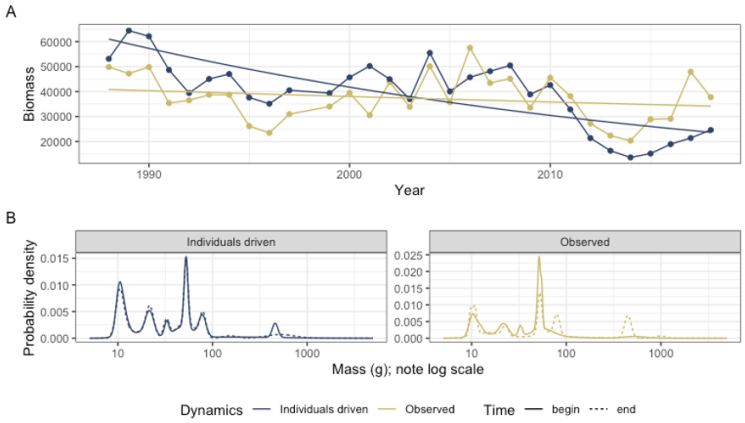

Figure 3-1. Illustration of individuals-driven (null model) dynamics as compared to observed dynamics (A), and the underlying dynamics of the ISD (B) for a sample route (Lindbrook, Alberta). A. Dynamics of total biomass. The gold points show the true values for total biomass in each year, and the blue points show the values for total biomass simulated from a null model that incorporates change in individual abundance, but assumes no change in the size structure, over time. The smooth lines show the predicted values from a Gamma (log-link) linear model of the form *total biomass = year * dynamics*, where *dynamics* refers to either the individuals-driven (null model) or observed dynamics. For this route, change in the individual size distribution has decoupled the dynamics of biomass from those that would occur due only to changes in individual abundance. The slope for individuals-driven dynamics is significantly more negative than for the observed dynamics (interaction term $p = 0.0013$). B. Underlying changes in the ISD. The individual size distributions for the first 5 years (solid lines) and last 5 years (dashed lines) of the timeseries. The x-axis is body size (as mass in grams; note log scale) and the y-axis is probability density from a Gaussian mixture model fit to a vector of simulated individual masses for all individuals observed in the years in questions, standardized to sum to 1. For the abundance-driven (blue) scenario, individuals' species identities (which determine their body size estimates) are re-assigned at random weighted by each species' mean relative abundance throughout the timeseries, resulting in a consistent individual size distribution over time. For the observed (gold) scenario, individuals' body sizes are estimated based actual species abundances at each time step. For this route, species composition has shifted over time and produced different ISDs for the "begin" and "end" time periods. Specifically, the "end" ISD has peaks at larger body sizes (ca. 90g and 500g) not present in the "begin" ISD. This redistribution of density towards larger body sizes results in an overall increase in body size community wide, which partially offsets declines in total biomass from those expected given change in individual abundance alone.

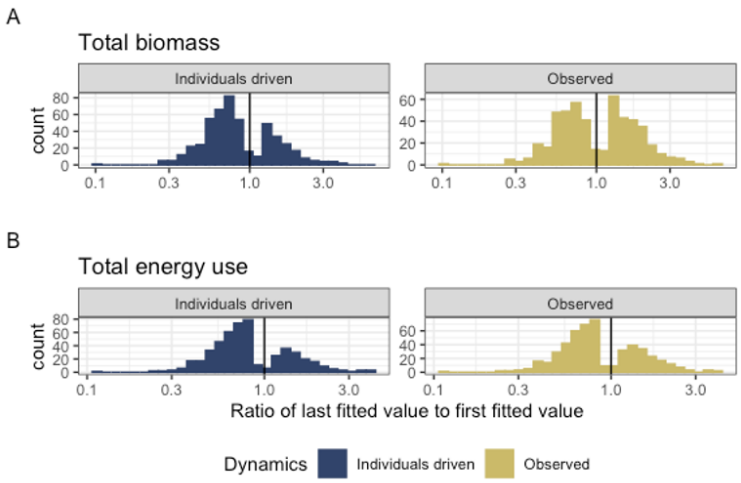

Figure 3-2. Histograms showing the direction and magnitude of long-term trends for the individuals-driven (null-model; left) and observed (right) changes in biomass (A) and energy use (B), for communities with a significant slope and/or interaction term (for biomass, 500/739 routes; for energy use, 509/739 routes; Table 3-1). Change is summarized as the ratio of the fitted value for the last year in the time series to the fitted value for the first year in the timeseries from the best-fitting model for that community. Values greater than 1 (vertical black line) indicate increases in total energy or biomass over time, and less than 1 indicate decreases. The individuals-driven dynamics (left) reflect the trends fit for the null model, while the observed dynamics (right) reflect trends incorporating both change in individual abundance and change in the size structure over time. For communities best-described by syndromes of "coupled trends" or "no directional change", the "individuals-driven" and "observed" ratios will be the same; for communities with "decoupled trends", there will be different ratios for or "individuals-driven" and "observed" dynamics.

Among routes with temporal trends ("coupled trends" or "decoupled trends"), there are qualitatively different continental-wide patterns in individuals-driven and observed dynamics for total biomass and total energy use. 70% of trends in individuals-driven (null model) dynamics for energy use are decreasing, and 67% for biomass (Table 3-2). For biomass, observed dynamics are balanced evenly between increases (49% of routes) and decreases (51%) - indicating that changes in the size structure produce qualitatively different long-term trends for biomass than would be expected given changes in individual abundance alone. However, trends for energy use (which scales nonlinearly with biomass) are dominated by decreases (35% of routes), more closely mirroring the trends expected given changes in individual abundance.

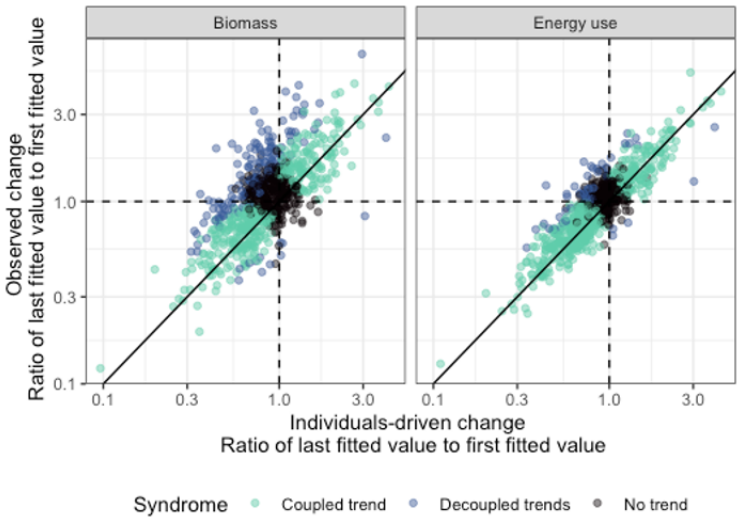

Figure 3-3. Observed change (ratio of last fitted value to first fitted value, y-axis) in total biomass (left) and total energy use (right) compared to the change expected only due to changes in the number of individuals (ratio of last fitted value to first fitted value from the null model dynamics, x-axis), for all routes (*n = 739*). Values greater than 1 (dashed horizontal and vertical lines) mark positive (increasing) trends, while values less than 1 are negative trends. Each point marks the fitted values from a Gamma log-link generalized linear model of the form *biomass = year * dynamics* or *energy use = year * dynamics* for a given route, which calculates separate long-term slopes for observed and individuals-driven dynamics. Points are colored corresponding to the syndrome of change identified for each route. Deviations from the 1:1 line (solid black line) reflect changes in the community size structure that modulate the relationship between individual abundance and total biomass or energy use. Changes in total biomass and total energy use generally track changes driven by fluctuations in individual abundance, with appreciable scatter around the 1:1 line. When this translates into a statistically detectable decoupling between observed and individuals-driven dynamics (a syndrome of "Decoupled trends"), this is usually in the form of individuals-driven change being more negative (a steeper decline or a smaller increase) than observed change in biomass or energy use (a less steep decline or larger increase), resulting in points falling above and to the left of the 1:1 line. This occurs more strongly and frequently for biomass than for energy use.

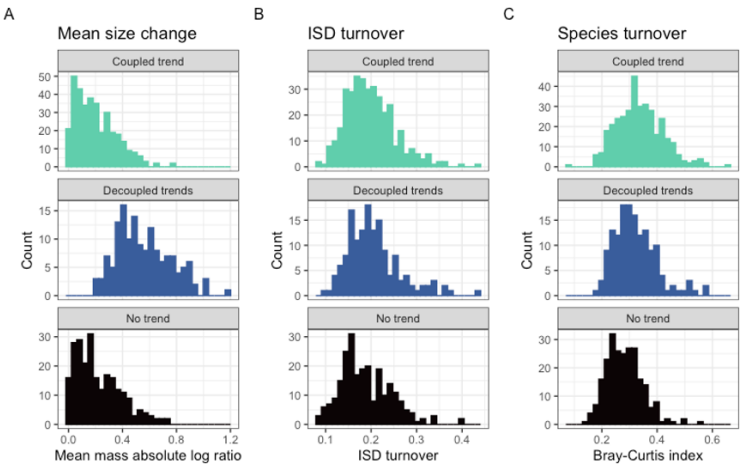

Figure 3-4. Histograms of (A) magnitude of change in mean body size from the first to the last five years of monitoring, (B) overall change in the size structure, and (C) change in species composition for routes whose dynamics for total biomass were best-described as syndromes of no directional change (bottom row; intercept-only model), decoupled trends for observed and individuals-driven dynamics (middle row), or coupled trends for observed and individuals-driven dynamics (top row). Change in mean body size (A) is calculated as the log of the ratio of the mean body size of all individuals observed in the last 5 years of the timeseries relative to the mean body size of all individuals observed in the first 5 years (see text). Overall change in the ISD (B) is calculated as the degree of turnover between the ISDs for the first and last five years of the timeseries (see text). Change in species composition (C) is characterized as Bray-Curtis dissimilarity comparing species composition in the first five years to the last five years.

Routes that exhibit decoupling between observed and individuals-driven changes in total biomass exhibit high magnitudes of change in mean body size (middle row, panel A) compared to the changes seen in routes that show either no trend or "coupled" trends (see also Appendix B). However, routes with all three syndromes of dynamics (coupling, decoupling, or no trend) are not detectably different in the degree of overall change in the ISD or in species composition over time (panels B and C; Appendix B).

3.6 Tables for Chapter 3

Table 3-1. Table of the number and proportion of routes whose dynamics for total biomass and total energy use are best described by the following syndromes: no directional change (intercept-only model, *biomass = 1* or *energy use = 1*); a coupled trend (*biomass = year* or *energy use = year*); or a model with decoupled temporal trends for observed and individuals-driven dynamics (biomass year * dynamics or energy use year * dynamics, where dynamics refers to observed or null model, individuals-driven dynamics).
31-32% of routes are best described as syndromes of "No directional change" (intercept-only models). For the remaining routes, in most instances, the dynamics of biomass and energy use exhibit a temporal trend, but with no detectable difference in the temporal trends for individuals-driven and observed dynamics ("Coupled trends"). However, for a substantial minority of routes (20% overall for biomass, or 30% of routes with a temporal trend; 7% overall for energy use, or 10% of routes with a temporal trend), there is a detectable deviation between the trends expected due only to changes in individual abundance and the observed dynamics ("Decoupled trends").

Currency	Syndrome	Number of routes	Proportion of routes
Total biomass	No directional change	239	0.32
Total biomass	Coupled trend	351	0.47
Total biomass	Decoupled trend	149	0.20
Total energy use	No directional change	230	0.31
Total energy use	Coupled trend	456	0.62
Total energy use	Decoupled trend	53	0.07

Table 3-2. The proportion of trends that are increasing (specifically, for which the ratio of the last fitted value to the first fitted value ¿ 1) for individuals-driven and observed dynamics, for routes exhibiting temporal trends ("coupled trends" or "decoupled trends") in total biomass and total energy use (for biomass, n = 500; for energy use, n = 509). Trends that are not increasing are decreasing.
Trends in individuals-driven dynamics are dominated by declines (67% of routes for total biomass, and 70% of routes for total energy). Observed dynamics for biomass differ qualitatively from the abundance-driven dynamics. Specifically, observed trends in biomass are evenly divided between increases and decreases (49% increasing). Observed trends in energy use more closely mirror individuals-driven trends (65% declines).

Currency	Proportion of increasing individuals-driven trends	Proportion of increasing observed trends	Number of routes with temporal trends
Total biomass	0.33	0.49	500
Total energy use	0.30	0.35	509

CHAPTER 4
EMPIRICAL ABUNDANCE DISTRIBUTIONS ARE MORE UNEVEN THAN EXPECTED GIVEN THEIR STATISTICAL BASELINE

4.1 Background

[*] Ecological communities are complex systems made of numerous interacting entities subject to a vast array of processes operating in different contexts and at different scales [64, 61, 69, 9, 80, 72]. One strategy for making sense of this inherent complexity is to identify patterns that occur consistently across many communities, and use these common phenomena to develop and test theories regarding general mechanisms that shape community structure [10, 69, 61, 39, 72]. Some of these patterns, however, can have counterintuitive emergent statistical properties [35, 36]. Left unexamined, these properties can confound the interpretation of the observed patterns: what we interpret to be the result of generative mechanism may be an artifact of statistical constraints. However, when these properties are properly understood and accounted for, they can provide leverage for detecting and identifying the processes at work in a system [55, 47].

The species abundance distribution (SAD) – the distribution of how all of the individuals in a community are divided among the species in that community – is a prime example of an ecological pattern that is both commonly invoked in the search for general processes, and subject to statistical constraints that have thus far complicated efforts to use it in this way [80, 74, 65]. The shape of the SAD is so consistent that it is often considered an ecological law [87, 89, 88, 91, 71, 74]. Across varied ecosystems and taxa, the species abundance distribution is dominated by a few very abundant species and a larger number of increasingly rare species, generating a distinctive hollow- or J-shaped curve when plotted with species rank on the x-axis and abundance on the y-axis [34, 74]. Community ecologists have used the SAD to test numerous theories regarding which biological processes are most important for structuring assemblages of species, by comparing theoretical predictions for the SAD to observed SADs [71, 74]. However, this approach has proven inconclusive because many theories predict similar shapes for the SAD [71, 74], and even experimental manipulations generate little variation in the shape of the SAD

[*]Reprinted with permission from Renata M. Diaz, Hao Ye, and S. K. Morgan Ernest, "Empirical abundance distributions are more uneven than expected given their statistical baseline", *Ecology Letters* 24 (2021), no. 9, 2025–2039.

[101]. Investigating and accounting for the statistical considerations that constrain the shape of the SAD may open up new avenues for ecological interpretations of the SAD.

In fact, the nearly ubiquitous shape of the SAD may transcend ecological processes and instead reflect mathematical properties inherent to abundance distributions. Complex systems across domains ranging from economics to information technology often exhibit empirical abundance distributions with hollow-curve forms similar to ecological SADs [98, 40, 80, 5, 56]. This suggests that the hollow curve is a common feature of abundance distributions and not necessarily an ecological phenomenon. Because the hollow-curve is observed in diverse systems and many theoretical generative processes converge to power-law or log-series abundance distributions (i.e. hollow curves) [90, 71, 80, 35, 36], approaches from statistical mechanics and complexity science may best explain the expected emergent shape for the distribution [90, 71, 80, 18]. Indeed, frameworks grounded in both entropy maximization (e.g. the Maximum Entropy Theory of Ecology; [45, 46]) and combinatorics (i.e. 'the feasible set'; [65]) generate realistic hollow curves via the random division of the total number of individuals in a community, N, into the total number of species present S. If the SAD is statistically inclined to be a hollow curve, the hollow-curve in itself may be of limited use for developing and testing ecological theories.

While SADs may be statistically constrained, this does not necessarily mean that they cannot be biologically informative. Biological factors may introduce subtle, but meaningful, deviations between observed SADs and the shapes of the SADs expected due to the mathematical constraints imposed by S and N, which we hereafter refer to as the "statistical baseline" [65, 47]. If the vast majority of mathematically achievable SADs for a community share a similar shape, an empirically observed SAD that deviates even slightly from this statistical baseline is unlikely to have emerged at random [65], and may be the signature of a non-random – i.e., biological – process operating on the relative abundances of species [47]. If, over many communities, there are consistent deviations between observed SADs and their statistical baselines, these deviations can help evaluate and refine ecological theories. For example, the high prevalence of rare species

in ecological communities has attracted considerable empirical and theoretical attention (e.g. [79, 67]), but it is unclear to what extent this phenomenon may derive from mathematical constraints on the SAD rather than ecological processes. If the prevalence of rare species in observed distributions consistently exceeds what would be expected to emerge from the statistical baseline, we would be prompted to look for ecological mechanisms promoting rarity. Candidate theories could then be evaluated based on how well their predictions for the rare tail of the SAD matched observed distributions. Thus, the deviations from the statistical baseline may enable us to detect strong ecological processes or evaluate theories [47, 119].

Successfully interpreting SADs in this fashion depends on our capacity to detect and quantify deviations between empirical observations and statistical baselines, which requires metrics and computational approaches that allow us to quantify and interpret whatever deviations may exist. Here, we build upon the combinatoric approach developed by [65] to define and explore statistical baselines for SADs. For a given N (total number of individuals) and S (total number of species), there exists a finite set of possible distributions of individuals into species. Collectively, this set of possible SADs is the feasible set, with each possible SAD constituting a single element of the set. If an observed SAD is drawn at random from the feasible set, it is likely to have a shape similar to the shapes most common in the feasible set. The feasible set therefore allows us to define statistical baselines for assessing deviations between observed SADs and what is likely to occur due to mathematical constraints [65].

The feasible set can also be used to explore how the characteristics of the statistical baseline, and the presence and nature of any deviations that occur, vary over ranges of values for S and N. Although most feasible sets are dominated by the hollow-curve shape, variation in S, N, and the ratio of N to S modulate the detailed attributes of the SADs in a feasible set [65]. For example, if the ratio of N to S is close to 1, all possible SADs are mathematically constrained to be fairly even [65]. Although an SAD that is very even would be highly unusual in most cases, it would be expected in this situation. The feasible set therefore allows us to appropriately calibrate our expectations for what types of observations would be surprising for an SAD given the specific

constraints imposed by its S and N. Additionally, accounting for variation in the specificity, or vagueness, of the expectations derived from the statistical baseline may be critically important for disentangling the aspects of the SAD that can be attributed to statistical constraints from those that result from other processes. If the vast majority of mathematically possible SADs are similar in shape – generating a very specific, narrowly defined statistical baseline – then even small deviations between an observed SAD and this baseline can signal the operation of ecological processes. However, if many different shapes occur with more even frequency in the feasible set, the statistical baseline is less specific and less well defined, and our sensitivity for distinguishing biological signal from statistical constraints is greatly reduced. This is more likely to occur when the size of the community, in terms of S and N, is small, because in such cases the feasible set may be too small for a particular shape to emerge as the most common shape. These statistical baselines with broad distributions may therefore impede our ability to assess whether observed deviations are ecologically generated or expected to emerge randomly [55]. This general concern has been acknowledged in efforts to compare ecological observations to statistical baselines [46, 116, 65] but there has not yet been a quantification of these effects for the SAD or an identification of the range of community sizes most strongly affected. Because ecologists study the SAD for communities varying in size from the very small – S and N < 5 – to the enormous – S and N $>> 1000$ – identifying the community sizes for which we can and cannot confidently detect deviations from the statistical baseline is necessary to appropriately contextualize our interpretations.

Here we use the feasible set to define statistical baselines for empirical SADs for 22,000 communities of birds, mammals, trees, and miscellaneous other taxa. We then compare observed SADs to their corresponding statistical baselines and evaluate 1) if the shapes of observed SADs consistently deviate from their statistical baseline, 2) how the characteristics and specificity of the statistical baseline vary over ranges of S and N, and 3) whether this variation appears to be associated with variation in our capacity to detect deviations between observations and the corresponding baselines.

4.2 Methods

Data and code for all of our analyses can be accessed at http://doi.org/10.5281/zenodo.4711104.

4.2.1 Datasets

We used a compilation of community abundance data for trees, birds, mammals, and miscellaneous additional taxa [116, 1, 2]. This compilation consists of cleaned and summarized community abundance data for trees obtained from the Forest Inventory and Analysis [118] and Gentry transects [85], birds from the North American Breeding Bird Survey [95], mammals from the Mammal Community Abundance Database [105], and a variety of less commonly sampled taxa from the Miscellaneous Abundance Database [1]. Because characterizing the random expectation of the SAD is computationally intractable for very large communities, we filtered our datasets to remove 4 communities that had more than 40714 individuals, which was the largest community we successfully analyzed. We further filtered the FIA database. Of the 103,343 communities in FIA, 92,988 have fewer than 10 species. Rather than analyze all these small communities, we randomly selected 10,000 small communities to include in the analysis. We also included all FIA communities with more than 10 species, which added 10,355 FIA communities to the analysis and resulted in a total of 20,355 FIA communities. Finally, for sites that had repeated sampling over time, we followed [116] and [2] and analyzed only a single, randomly selected, year of data, because samples taken from a single community at different time points are likely to covary. It should be noted that our analyses include data from the Mammal Community Database and Miscellaneous Abundance Database that were collected over longer timescales and cannot be disaggregated into finer units of time. Our final dataset consisted of 22,000 communities with S and N ranging from 2 to 250 and 4 to 40714, respectively (Figure 4-1). Details and code for the filtering process can be found at https://doi.org/10.5281/zenodo.4744720.

4.2.2 Accounting for empirical sampling error

Because it is logistically impossible to exhaustively census all individuals present in most empirical systems, SADs derived from field sampling will inevitably be subject to some degree of

sampling error [6]. Therefore, in addition to analyzing the raw SADs in our database, we employed two resampling schemes to test if, and how, different forms of observation error affect our results.

First, we explored the possibility that empirical sampling systematically undercounts the true number of rare species in a community [87, 42]. Rare species are more likely to escape detection during sampling, leading to an underestimate of both the total species richness of a community and the proportion of species in the rare tail of the SAD [87]. We used a procedure based on species richness estimators to adjust for this possibility (see also [107] for the use of richness estimators to distinguish between completely and incompletely censused communities). We computed the estimated richness for each community using the bias-corrected Chao and the ACE estimators (as implemented in the R package *vegan*; [81, 13, 82]. To each of these richness estimates, we added one standard deviation of the estimate, and then took the mean of the two results. This yields a generous estimate of the true number of species in the system. If this estimate exceeded the observed species richness, we added the missing species each with abundance 1. These adjusted SADs allowed us to explore the consequences of undersampling rare species while making the smallest possible changes to S and N.

Second, we tested the sensitivity of our results to sampling variability across all species in the SAD – not just rare species - using subsampling. For each observed community, we constructed subsamples by randomly drawing 60% of the observed number of individuals from the total pool of individuals in the community, without regard to species and without replacement. The precise proportion of individuals drawn in each subsample should not dramatically affect the qualitative outcome. We selected 60% so as to introduce appreciable room for sampling error between the raw and subsampled SADs, but to produce subsampled SADs with N (and presumably S) in a comparable size range to the raw ones. Extremely small subsamples (e.g. 10%) could introduce complications related to small N and S that could obscure the effects of sampling error, while very large subsamples (e.g. 90%) could recapture the raw distributions too closely to be informative. We generated 10 resampled communities for each observed community.

We ran our computational pipeline using all raw SADs and all SADs adjusted for undersampling of rare species. Because the subsampling approach increased computational effort approximately tenfold, we analyzed all subsampled communities for the Mammal Community, Miscellaneous Abundance, and Gentry databases, but only a random subset of 300 (of 2773) communities from the Breeding Bird Survey and 2000 (of 20179) from the FIA – 1,000 with S $<$ 10, and 1,000 with S $>=$ 10.

4.2.3 Generating the statistical baseline

We use the concept of the "feasible set" to establish a statistical baseline for the SAD [65]. For a given number of individuals N, there are a finite number of unique ways to partition those individuals into S species. The complete set of these unique partitions is the feasible set. In this approach, neither species nor individuals are distinguishable from each other; thus partitions are unique if and only if they differ in the number of species that have a particular abundance [65]. Operationally, this means that for S = 3 and N = 9, the SADs (1, 3, 5) and (2, 2, 5) count as distinct partitions, but (1, 3, 5) and (3, 1, 5) do not, because they each contain one species with an abundance 1, 3, and 5, respectively, and differ only in the order of the numbers. In the absence of justification for additional assumptions regarding the distinguishability of species and/or individuals, we adopted this simple set of assumptions that has previously been shown to generate realistic statistical baselines [65].

While it is possible to list all possible partitions in the feasible set for small S and N, the size of the feasible set increases rapidly with S and N. An exhaustive characterization of the statistical properties of the feasible set for large S and N quickly becomes computationally intractable. This renders it necessary to draw samples from the feasible set, rather than enumerating all of its elements. Previous efforts in this vein [65] have been constrained by the problem of unbiased sampling of large feasible sets. We developed an algorithm to efficiently and uniformly sample feasible sets even for large values of S and N. In brief, the algorithm takes a generative approach to sample the feasible set for a given combination of S and N, based on recurrence relations used to calculate the size of the feasible set. Let $f(S,N)$ be the number of

possible partitions of N individuals into exactly S species, i.e. the size of the feasible set for given values of S and N. Computation of $f(S,N)$ can be achieved without enumerating the entire feasible set through the recurrence relation $f(S,N) = f(S-1,N-1) + f(S,N-S)$ (originally documented in a 1742 letter from Euler to Bernoulli; [30]). For example, consider the feasible set with S = 3 and N = 7. For all possible partitions, either (a) at least one species has an abundance equal to 1, or (b) all of the species have abundance greater than 1. In the case of (a), removing one species with abundance equal to 1 must result in a partition of 6 individuals into 2 species. In fact, all of the unique partitions in (a) must have a corresponding unique partition in the feasible set for S = 2 and N = 6, and vice versa. In the case of (b), removing 1 individual from each species must result in a partition from the feasible set with S = 3 and N = 4. Here, all the partitions in (b) must have a corresponding unique partition in the feasible set with S = 3 and N = 4, and vice-versa. Therefore, $f(3,7) = f(2,6) + f(3,4)$. By storing the values in a lookup table, $f(S,N)$ can be calculated for increasing values of S and N through straightforward summation.

This recurrence relation also makes it possible to draw random samples from the feasible set without enumerating all possible partitions of N into S. For the example of S = 3 and N = 7, there are a total of 4 possible partitions (i.e. $f(S,N) = 4$). Because $f(2,6) = 3$ and $f(3,4) = 1$, we know that (a) 3 of the 4 partitions must correspond to a partition of the feasible set with S = 2 and N = 6 (but with a species of abundance equal to 1 removed), and (b) 1 of the 4 partitions must correspond to a partition of the feasible set with S = 3 and N = 4 (but with 1 individual removed from each species). Thus, we can determine the probability that a partition drawn at random from the feasible set for S = 3 and N = 4 is in case (a) – probability $\frac{3}{4}$ - or case (b) – probability $\frac{1}{4}$. To generate a partition in case (a), we sample a partition for S = 2 and N = 6 and then add a species with abundance equal to 1; for case (b), we sample a partition for S = 3 and N = 4 and then add 1 individual to each species. In this way, we use the recurrence relation to transform the problem of sampling from a large feasible set into the problem of sampling from a smaller, different feasible set. This procedure continues until a partition is uniquely determined, after which some back-transformation yields a unique partition for the feasible set of interest. A detailed

description of the algorithm we use, based on a slightly different recurrence relation, is available at https://doi.org/10.5281/zenodo.4744720 and is implemented in the R package *feasiblesads* available at http://doi.org/10.5281/zenodo.4710750.

For every community in our database, we drew 4000 samples from the feasible set to characterize the distribution of statistically probable shapes for the SAD. We filtered the 4000 samples to unique elements. For small values of S and N, it can be impossible or highly improbable for the 4000 samples from the feasible set to all be unique, but for large communities, all 4000 are usually unique. We refer to this as the sampled feasible set.

4.2.4 Comparing observed SADs to their statistical baselines

We compared SADs to their statistical baselines using several metrics, including a general measure of dissimilarity, as well as skewness, Simpson's evenness, Shannon's index, and the proportion of rare species (species with abundance = 1). These metrics represent just a few of the vast array of possible summary metrics to describe the shape of the SAD, each of which emphasize different aspects of the distribution. In this first effort to compare empirical distributions to a statistical baseline, we selected a suite of complementary metrics and explored whether our overall results were consistent between metrics. By calculating these metrics for each the community's sampled feasible set (see Generating the statistical baseline, above), we generated a portfolio of measures describing the shapes expected from randomly sampled SADs.

First, as a general characterization of whether observed SADs have rare or common shapes relative to their feasible sets, we computed a dissimilarity score comparing SADs to the central tendencies of their feasible sets (following [65]). We defined the degree of dissimilarity between two SADs with the same S and N as the proportion of individuals allocated to species with different abundances between the two SADs, calculated as $\frac{\sum_{i=1}^{S} n1_i - n2_i}{2N}$ where $n1_i$ is the abundance at rank i for one SAD and $n2_i$ is the abundance at rank i for the other SAD. This value ranges from 0 to 1, with 1 being high dissimilarity. To find the central tendency of a given sampled feasible set, we identified the sampled SAD with the lowest mean dissimilarity compared to the rest of the SADs in the feasible set. We calculated the dissimilarity between every sample drawn

from the feasible set and a random set of 500 other samples, using a subset of samples for comparisons because it is computationally impractical to make all pairwise comparisons between large numbers of samples. To assess whether an observed SAD was highly dissimilar to its central tendency, we calculated the degree of dissimilarity between the central tendency of the corresponding feasible set and all other samples from that feasible set, and between the central tendency and the observed SAD. Although the dissimilarity score is scaled from 0 to 1, the distributions of dissimilarity scores for samples from the feasible set can vary over broad ranges in S and N. We therefore used the percentile rank of the observed dissimilarity scores, relative to the distribution of dissimilarity scores from the corresponding sampled feasible sets, to quantify how likely or unlikely observed dissimilarity scores are across the range of S and N in our datasets. For a single community, an observed percentile score of 95 indicates that there is a 5% chance of drawing a value greater than the observed value from the distribution of values from the sampled feasible set. Aggregating across communities, if observed SADs reflect random draws from their feasible sets, their percentile rank values should be uniformly distributed from 0 to 100. However, if observed SADs are consistently more dissimilar to their feasible sets that expected at random, the percentile values will be disproportionately concentrated at high values. We used a one-tailed 95 confidence interval and tested whether the percentile values for the dissimilarity scores of observed SADs fell above 95 more than 5% of the time. We note that it is impossible for an observation fall above the 95th percentile if there are fewer than 20 values in the sampled distribution. We therefore excluded from this analysis communities with fewer than 20 unique SADs in their feasible sets, yielding a total of 22,490 communities. Finally, note that, if the observed dissimilarity scores for individual communities are not systematically higher than the distributions of dissimilarity scores from the corresponding feasible sets, increasing the number of communities in the analysis will not increase the frequency of extreme percentile scores.

While the degree of dissimilarity between SADs and the central tendency of the feasible set provides an overall sense of deviations among possible SADs, it does not describe how observed SADs may differ from their feasible set. We therefore used a set of more targeted, ecologically

interpretable metrics to explore how observed SADs compare to their feasible sets in their shape and proportion of rare species. We examined three metrics for the shape of the SAD - skewness, Simpson's evenness (1-D), and Shannon's index. Skewness measures the asymmetry of a distribution around its mean. The Simpson and Shannon indices are commonly used metrics for assessing how equitably abundance is distributed across species [70]. We also calculated the proportion of rare species (species with abundance = 1) in each SAD, because the proportion of rare species in a community is comparable across different community sizes and is of special interest to ecologists.

As with the degree of dissimilarity score, to assess whether the shape of an observed SAD was statistically unlikely, we used percentile ranks to compare the observed values of the summary metrics to the distributions of values for those metrics obtained from each community's sampled feasible set. The actual ranges and values of summary metrics vary widely over the ranges of S and N in our data and thus cannot directly compared, but percentile ranks are comparable across different community sizes and allow assessment across our entire dataset. We used two-tailed 95% intervals to test whether observed communities' percentile values for each metric were disproportionately concentrated below 2.5 or above 97.5. In all cases, in testing for unusually high percentile scores, we defined the percentile score as the proportion of values in the sampled distribution strictly less than the observed value, while in testing for low values, we defined it as the proportion of sampled values less than or equal to the observed value. This ensured a conservative estimate of how extreme the observed values were relative to the sampled distribution. Because it is impossible for an observed percentile score to be above or below the 97.5th or 2.5th percentile if there are fewer than 40 values in the sample distribution, we excluded from these analyses communities with fewer than 40 SADs in their feasible sets. Finally, note that skewness, as implemented in the R package *e1071* [76], always evaluates to 0 for distributions with only two species, and we therefore excluded those cases from analyses of skewness. Our final analysis included 21,395 communities for skewness and 21,403 communities for all other shape metrics.

4.2.5 The narrowness of the expectation

We also used the distributions of dissimilarity scores and shape metrics to quantify the relative specificity of the statistical baseline, in order to assess when there could be challenges in determining whether observed communities differ from their statistical baselines. For an overall sense of how tightly elements of the feasible set were clustered around its central tendency, we calculated the 95th percentile of dissimilarity scores for all samples from a feasible set compared to the central tendency of that feasible set. This value shows how dissimilar to the central tendency an observed SAD would need to be to count as "extreme" relative to the feasible set. For the shape metrics, we calculated a breadth index defined as the ratio of the range of values encompassed within a two-sided 95% density interval relative to the full range of values in the distribution (Figure 4-2). This breadth index for the statistical baseline ranges from 0 (a very narrow distribution and well-resolved baseline) to 1 (a very broad distribution), and is comparable across feasible sets for varying combinations of S and N. These approaches correspond qualitatively to more computationally-intensive approaches to measuring the self-similarity of the elements of feasible sets (see https://doi.org/10.5281/zenodo.4744720). We explored how the narrowness of the statistical baseline varies with the size of the feasible set and the ratio of N to S.

4.3 Results

Comparing observed SADs to their statistical baselines For four of the five datasets we analyzed – BBS, Gentry, Mammal Communities, and Miscellaneous Abundance – observed SADs are more dissimilar to their statistical baselines than would be expected by chance (Figure 4-3). Combined over these four datasets, 29% of observed SADs are more dissimilar to the central tendency than are 95% of samples from the corresponding feasible sets (Table 4-1). If observed SADs reflected random draws from the feasible set, we would expect only 5% to be that dissimilar. These highly unlikely SADs have dissimilarity scores from 1.007 to 6.3 times the 95th percentile of dissimilarity scores comparing the central tendency to samples from the feasible set, an absolute increase ranging from .001 to .54 on a scale from 0-1 (see https://doi.org/10.5281/zenodo.4744720). These datasets also contain highly unlikely observed

SADs in terms of their shape metrics. At random, roughly 2.5% of observed percentile scores for these metrics should be very high (¿97.5) or very low (¡2.5). Compared to their feasible sets, these four datasets contain a disproportionate number of communities with very low values for Simpson's evenness and Shannon diversity, and very high skewness, relative to their feasible sets (Table 4-1). The Mammal Community and Miscellaneous Abundance databases also have high proportions of rare species, but this tendency is weaker for BBS and nonexistent for Gentry – in fact, the Gentry dataset has a high representation of sites with low proportions of rare species (20% of sites; https://doi.org/10.5281/zenodo.4744720). The Gentry dataset also has a disproportionate number of communities with the opposite tendencies to the other datasets for the other shape metrics– i.e., an overrepresentation of communities with high Simpson's evenness and Shannon diversity, and low skewness.

In contrast to the other datasets, percentile scores for sites from the FIA dataset are more uniformly distributed, and the proportions of extreme values are closer to what would be expected by chance (Figure 4-3, Table 4-1). Only 7% of FIA communities are highly dissimilar to their feasible sets (compared to a random expectation of 5%). Among the shape metrics, only 2.8% (compared to 2.5% at random) of sites have high values for skewness, 1.3% have high proportions of rare species, 5.7% have low Simpson's evenness, and 5.4% have low Shannon diversity.

4.3.1 The narrowness of the expectation

The ability to detect deviations from the statistical baseline depends in part on the distribution of SADs in the feasible set. Overall, as the size of the feasible set increases, the SADs in a feasible set become more narrowly clustered around the central tendency of that feasible set, and the sampled distributions for shape metrics generally become less variable (Figure 4-4). In small communities, the breadth indices are highly variable and often very large – approaching 1, meaning that a 95% density interval of the values in the distribution spans nearly the entire range of values – while the breadth indices for larger communities rarely exceed 0.7 for skewness, Simpson evenness, and Shannon diversity, and .8 for the proportion of rare species. Among our datasets, the FIA and Mammal Community databases have the smallest communities, in terms of

S and N, and tend to have the largest proportions of feasible sets with high breadth indices (https://doi.org/10.5281/zenodo.4744720).

4.3.2 Sensitivity to sampling variability

In almost all cases, SADs adjusted for the under-observation of rare species are even more extreme relative to their feasible sets than unadjusted SADs (Figure 4-5; see https://doi.org/10.5281/zenodo.4744720 for complete archival results of resampling). For all datasets, adjusted SADs show more high values for skewness and the proportion of rare species, and low values for Simpson's evenness and Shannon diversity, than unadjusted SADs.

Subsampling consistently reduces the proportion of extreme observations across all datasets and metrics (Figure 4-5; https://doi.org/10.5281/zenodo.4744720). In most instances, the proportion of extreme observations still exceeds the proportion that would be expected by chance. However, the proportion of sites with high numbers of rare species observed for the BBS and Mammal Community databases drop from 4.5% to 1% and 13% to 3.5% with resampling. For FIA, the proportions of sites with high dissimilarity, low evenness and Shannon diversity all drop from 6-8% to 2-3%. Note that, for FIA, neither the raw nor the resampled SADs have a disproportionate representation of extreme values for the remaining metrics.

4.4 Discussion

We found widespread evidence that SADs for a range of real ecological communities deviate from the forms expected given the distribution of shapes within their feasible sets. Overall, these deviations may signal that ecological processes operate on top of statistical constraints, thereby driving the SAD away from shapes generated by purely statistical processes. We also found that the magnitude and form of deviation varied among the datasets we considered. This variability may reflect statistical phenomena related to the size of S and N and their ratio, or it may reflect different biological processes dominating in different contexts. Finally, although a disproportionate number of communities deviated statistically from their feasible sets, there were also many communities for which we did not detect deviations. This does not imply the absence of ecological processes operating on these SADs. Rather, one possible explanation is that

multiple ecological processes are operating simultaneously and with countervailing effects, resulting in no dominating net impact on the shape of the distribution beyond that imposed by fundamental constraints [46, 47]. Going forward, testing whether ecological theories or common functional approximations (e.g. the log-normal distribution) accurately predict the deviations between observed SADs and their statistical baselines may be much more fruitful than focusing only on the general form of the SAD [74, 65, 47].

In most cases, and most pronouncedly for the Breeding Bird Survey, Mammal Community, and Miscellaneous Abundance databases, our results suggest that the prevailing processes cause abundance distributions to be highly uneven, rather than those that produce more even abundances across species. For these communities, observed SADs tended to be unusually skewed and uneven, and to have a high proportion of rare species, compared to their feasible sets. Accounting for undersampling of rare species strengthened these effects, while subsampling weakened them. Perhaps unsurprisingly, the effect of these two resampling approaches was especially noticeable for the proportion of rare species; enriching the SAD directly adds rare species, while subsampling is likely to drop rare species even if it otherwise recaptures the general shape of a distribution. The long tail of rare species in the SAD has been a consistent focus in SAD research, and our results highlight that the rare tails of observed SADs are extraordinary, even among the hollow-curve shapes that dominate the feasible set. Ecological processes may lengthen the rare tail and decrease the evenness of the SAD, for example by promoting the persistence of rare species at very low abundances [122]. Or, they could drive abundant species to have larger populations than would be statistically expected, without also driving other species entirely to extinction [12].

While the Gentry database also exhibits deviations tending towards high unevenness, an even greater proportion of its communities are more even, and have a lower proportion of rare species, than would be expected given their feasible sets. This could indicate that there are biological differences between the systems in the Gentry and other datasets that result in different forms for the SAD. Alternatively, the statistical characteristics of the feasible sets for these

communities could modulate the detected deviations. Communities in the Gentry database have high species richness and low average abundance (Figure 4-1). Among these, many of the communities exhibiting high evenness and low proportions of rare species are those with very high species richness and low average abundance ($\frac{N}{S} < 3$ (see https://doi.org/10.5281/zenodo.4744720). As a result, these communities have unusual statistical baselines: for example, the corresponding feasible sets have the highest proportions of rare species of any of the feasible sets in our analysis. Although observed SADs for these communities also have high proportions of rare species, taking the statistical baseline into account would suggest that the extraordinary thing about these SADs is that they do not have even more rare species. Simultaneously, there may be biological reasons why the species-rich but relatively low-abundance tropical tree communities of the Gentry database differ from those in other datasets. The same mechanisms that promote high diversity may manifest in high evenness, and/or ecological features particular to these forests may produce unusual shapes for the SAD. Because no communities from our other datasets are comparable in S and N, we cannot disentangle these statistical and biological explanations. This is an excellent opportunity to develop additional theoretical and empirical approaches to predict and explain variation in the deviations between SADs and their feasible sets, in particular for species-rich communities across ecosystems.

Unlike the other four datasets, communities in the FIA dataset showed weak or no evidence of deviations from their feasible sets. We entertained two general classes of explanation for why the FIA dataset differs from the others in our analysis: first, that biological attributes of the FIA communities cause the SADs for these communities to differ from the others in our database, and second, that statistical phenomena related to S and N may modulate the capacity to detect deviations for these communities. To distinguish between possible biological drivers causing FIA to differ from the other datasets, and factors intrinsic to S and N, we compared a subset of 300 FIA communities to communities from other datasets with directly matching S and N. We did not find differences in the distribution of percentile scores for any metrics between communities from

FIA and communities from other datasets, confirmed via Kolmogorov-Smirnov tests (see archival analyses at https://doi.org/10.5281/zenodo.4744720). Although 300 communities constitute a small sample relative to the 20,355 FIA communities we analyzed, these results point to statistical phenomena, and not biological attributes unique to FIA, as the likely explanation for the differences. A second possibility is that these differences reflect statistical phenomena related to community size in terms of S, N, and as a result, the number of possible SADs in a community's feasible set. The FIA communities are the smallest across our datasets (Figure 4-1), and communities with small values of S and N have smaller feasible sets. When there are relatively few possible SADs in the feasible set, they may be less tightly clustered around their central tendencies, and the distributions for their shape metrics may be less narrowly peaked, than when there are very large numbers of possible SADs. High variability within the feasible set weakens the statistical distinction between "common" and "extreme" shapes (Figure 4-2). Under these circumstances, any deviations – or lack thereof – will be less informative than for communities with more strongly defined statistical baselines [55]. The dissimilarity to the central tendency, and the distributions of breath indices for specific metrics, broadly align with this principle. Across the range of community sizes represented in our datasets, small feasible sets have highly variable, and often very broad, feasible sets (Figure 4-4). More specifically, very small communities – for example, those with fewer than 2000 possible SADs in their feasible sets, or S approximately = 20 and N approximately = 40 – exhibit more highly variable feasible sets than large communities, and these small communities also show less consistent deviations (Figure 4-6; https://doi.org/10.5281/zenodo.4744720). Of our datasets, FIA is most dominated by small communities (68% of communities have fewer than 2000 possible SADs), and these small-community phenomena may therefore have the greatest impact on results aggregated over the FIA dataset.

If it is true that the highly variable feasible sets associated with small communities contribute to the weak evidence of deviations observed for the FIA dataset, such considerations affect our capacity to use this approach to distinguish signal from noise for a substantial

contingent of ecological communities. Because the combinations of S and N represented in our analyses are irregularly distributed among different datasets (Figure 4-1), and because there is a great deal of variation in our breadth indices not accounted for by the size of the feasible set (Figure 4-4), we do not interpret these results as showing a threshold for defining problematically small communities. A more systematic exploration of the S and N state space, combined with more nuanced metrics for characterizing the variability of the feasible set, could clarify the relationship between S and N, the size of the feasible set, and statistical power. However, FIA and other small, highly variable communities have on the order of 10-20 species and 30-60 individuals, suggesting a general range of values below which we have diminished power to detect deviations from the statistical baseline represented by the feasible set. Communities with on the order of 5 species, or 100s to 1000s of individuals, have previously been suggested as "small" in this context [87, 74]. To meaningfully draw inferences using deviations in these small communities, we will need more sensitive metrics than those used here, and/or theories that generate more specific predictions for the SAD. In the absence of such, we may stand to learn the most by focusing on SADs from relatively large communities.

It is also important to recognize that there are multiple plausible approaches to defining a statistical baseline for the SAD, of which we have taken only one [43, 65]. Our approach follows [65] and reflects the random partitioning of individuals into species, with the resulting distributions considered unique if the species' abundance values are unique, regardless of the order in which the values occur. This philosophy reflects a longstanding approach in the study of abundance distributions: to focus on the shape of the distribution without regard to species' identities [74]. Other assumptions regarding the statistical baseline may be equally valid and generate different statistical expectations, which may alter if, and in what ways, empirical distributions appear unusual. For example, incorporating differences in species order into the statistical baseline – which would imply that identifying which species contain the most or least individuals is important – might reduce the representation of long-tailed, highly uneven SADs within the feasible set, and make the rare tail observed for real SADs appear more unlikely than it

does here. Under our assumptions, the SADs (1,2,3,4) and (1, 1, 1, 7) each count as only one unique SAD. Taking species order into account would mean that (1,2,3,4) would count as 24 (4!) unique SADs, because there are 4! ways to assign the abundances to each species. However, an SAD containing species with equal abundances, such as (1, 1, 1, 7), would only count as 4 unique SADs. For SADs, equal abundances are likely most prevalent among rare species. If this is true, then this set of assumptions would generate feasible sets where rare-tailed SADs are relatively scarce, making observed SADs with rare tails seem even more extraordinary. Additional formulations for the statistical baseline exist, including those that approximate exponential, Poisson, or log-series distributions in the limit [45, 31]. Investigating and comparing the results that emerge from different baselines will be an important next step towards reinvigorating the use of the SAD as a diagnostic tool.

Our study demonstrates the utility, and the potential challenges, of applying tools from the study of complex systems and statistical mechanics to the study of ecological communities [43, 46, 116, 47]. While concepts such as maximum entropy and the feasible set are promising horizons for macroecology, the small size of some ecological communities may present difficulties that are rare in the domains for which these tools were originally developed [55, 43]. When the observed numbers of species and individuals are too small to generate highly resolved statistical baselines, these approaches will be less informative than we might hope – as appears to be the case for the smallest communities in our analysis. In larger communities, where mathematical constraints have more resolved effects on the form of the SAD, our results show that these constraints alone do not fully account for the extremely uneven SADs we often observe in nature – leaving an important role for ecological processes. This ability to detect and diagnose the specific ways in which empirical SADs deviate from randomness can generate new avenues for understanding how and when biological drivers affect the SAD. There are, of course, still many elements to be improved in our ability to distinguish biological signal from randomness, including assessing alternative statistical baselines and calibrating our expected power to detect deviations, especially for small communities. Indeed, more sensitive metrics could also enable identification

of processes that operate through time. Continuing to explore and account for the interplay between statistical constraint and biological process constitutes a promising and profound new approach to our understanding of this familiar, yet surprisingly mysterious, ecological pattern.

4.5 Figures for Chapter 4

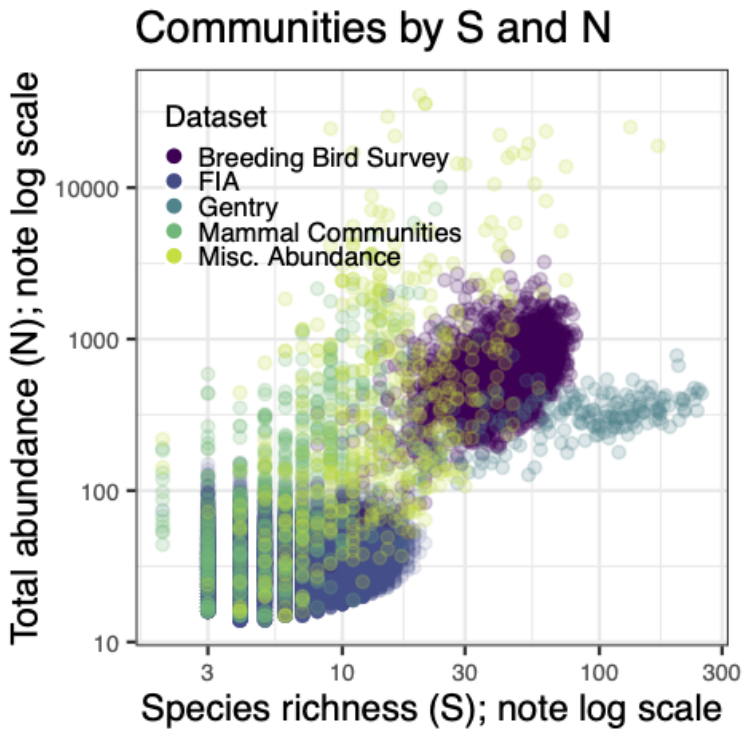

Figure 4-1. Distribution of communities from each dataset in terms of total abundance (N) and species richness (S). Communities range from few species and individuals (lower left corner) to speciose communities with many individuals (upper right). However, datasets are not evenly distributed across this state space due to differences in their sampling intensity, design, and underlying biology (e.g. productivity, regional richness, taxonomic group, or other factors that influence the capacity of a community to support large numbers of species and individuals). In particular, note that the FIA dataset comprises very small communities, and communities from the Gentry dataset are extreme in both their high species richness and low average abundance.

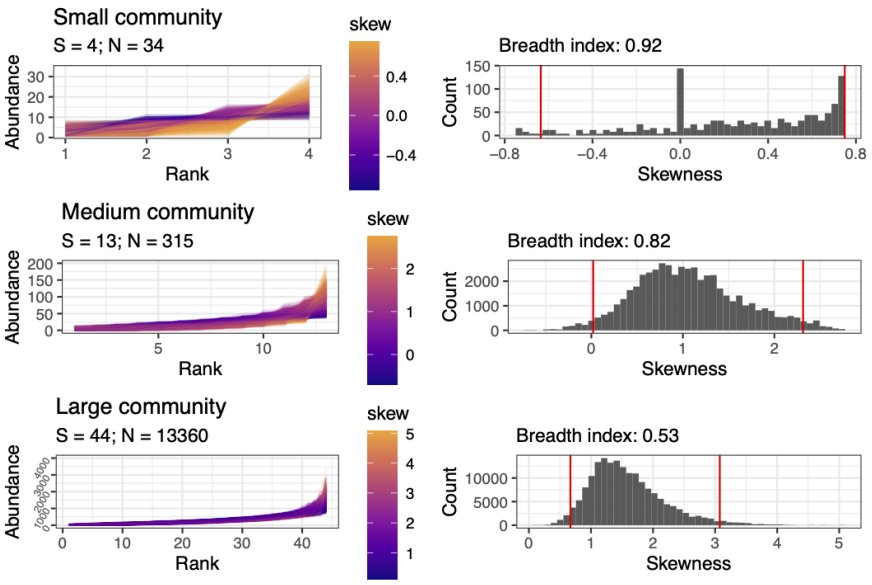

Figure 4-2. Large feasible sets may allow better detection of deviations from the statistical baseline by generating more specific, narrowly-defined baselines. We illustrate this phenomenon using 3 hypothetical communities: a small community (S = 4, N = 34; top row), an intermediate community (S = 13, N = 315; middle row), and a large community (S= 44, N = 13360; bottom row). The large communiity has approximately 6.59e+70 possible SADs in its feasible set, while the intermediate community has 1.001e+12 and the small community has only 297. For every SAD sampled from the feasible set (left column), we calculate the skewness (color scale) or other summary metrics (not shown). The distributions of these values (right column) constitute the statistical baseline. We define a "breadth index" as the ratio of the range encompassed in the two-tailed 95% density interval (distance between red lines, right), compared to the full range of values for the statistic (distance between the maximum and minimum values). As S and N increase, the size of the feasible set increases, resulting in a narrower statistical baseline (smaller breadth index) – thus enabling easier detection of deviations that may be the result of ecological processes affecting the SAD.

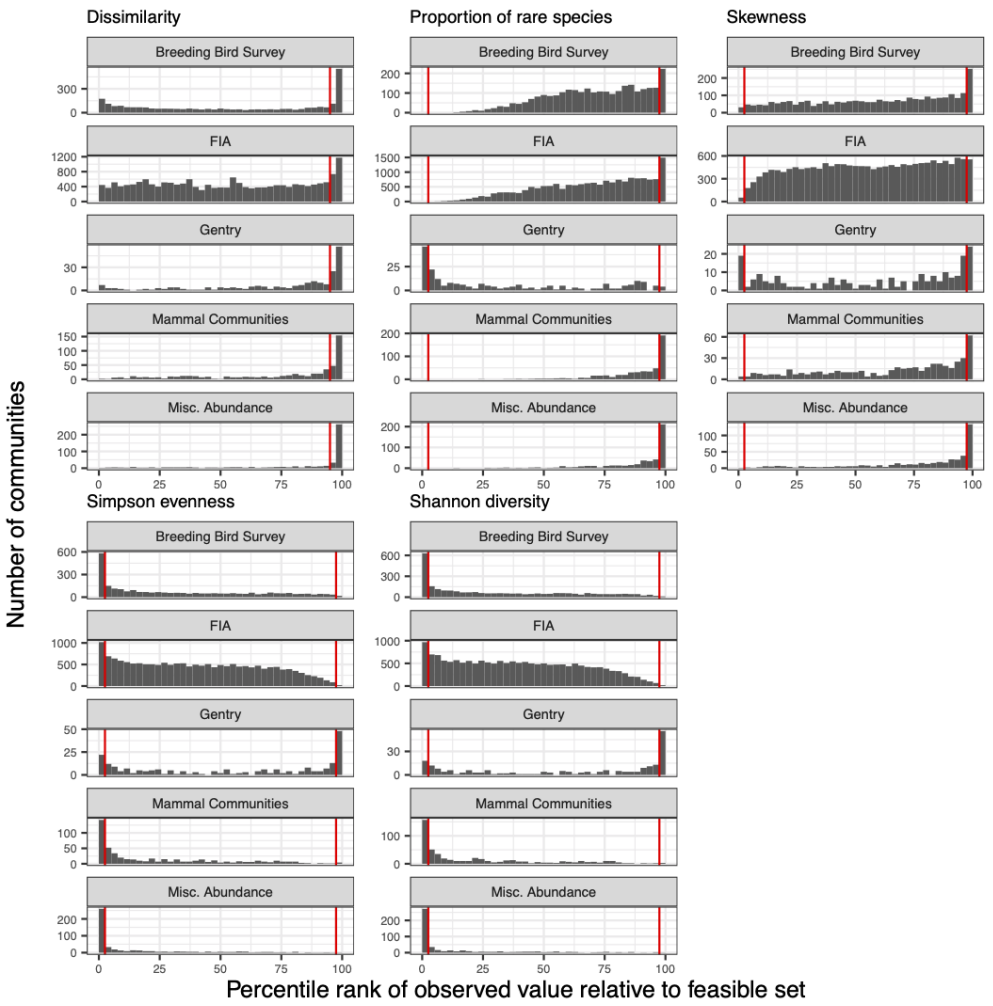

Figure 4-3. Many ecological communities are highly unusual compared to their statistical baselines. Percentile ranks are calculated by comparing each community to its sampled feasible set, with very high or very low percentile ranks reflecting extreme values relative to statistical baselines. The vertical red lines mark the 95th percentile for the dissimilarity to the central tendency, and the 2.5th and 97.5th percentiles for all other metrics. Species abundance distributions that are sampled at random from the feasible set will produce percentile ranks that are roughly uniformly distributed from 0 to 100, with approximately 5% of values above the 95th percentile or 2.5% of values above and below the 2.5th and 97.5th percentiles, respectively. In contrast, most datasets have more communities that are highly skewed or uneven than would be expected by chance. The percentile values shown are the mean of the percentile scores defined as the proportion of comparison values $<=$, and $<$, the focal value. In calculating the proportion of sites with extreme values, the $<=$ designation gives an appropriately conservative estimate of the proportion of high values, but overestimates the proportion of very low values, and the reverse occurs for the $<$ designation.

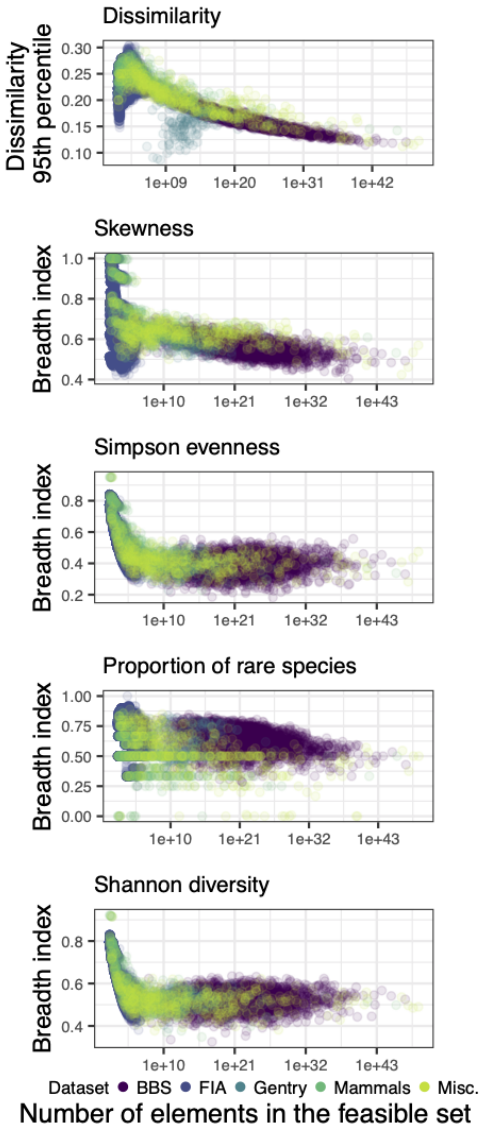

Figure 4-4. The variability of the feasible set, defined as either the 95th percentile of dissimilarity scores comparing elements of a feasible set to the central tendency of that feasible set, or via a breadth index (see Figure 4-2), decreases as the number of possible SADs in the feasible set becomes very large. Highly variable feasible sets constitute broad, poorly-defined statistical baselines that may impede our ability to confidently detect deviations between observations and what is expected given the baseline. Small feasible sets, which occur for small combinations of S and N, are often highly variable. The majority of these small, highly variable feasible sets occur for communities in the FIA and Mammal Community databases. Although the Gentry dataset also contains communities with small feasible sets, these communities also have a very low ratio of N to S, meaning their entire feasible sets may be constrained to be more self-similar than small feasible sets in general (see Dissimilarity to central tendency). There is, however, substantial additional variation in the dissimilarity and breadth indices not accounted for by the size of the feasible set or the ratio of N to S.

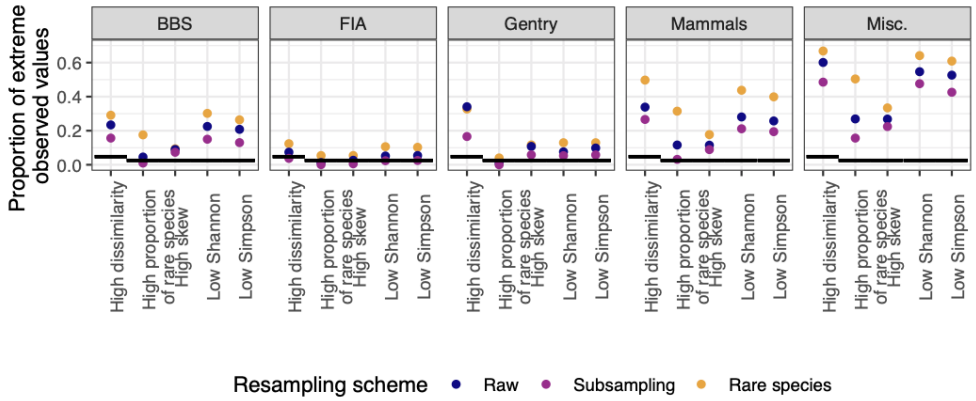

Figure 4-5. Summaries of how resampling to adjust for under-detection of rare species (orange) and subsampling (pink) change the proportion of extreme values observed for each metric and dataset. The horizontal black lines mark the approximate proportions of extreme values that would be expected at random: 5% for dissimilarity to the central tendency, and 2.5% for all other metrics. Adjusting for rare species consistently increases the proportion of extreme values relative to the raw SADs, while subsampling often decreases it but generally does not eliminate or change the direction of the effect. The exception is for the FIA dataset, which does not show strong deviations for either raw or resampled SADs. Shown are the effects and directions observed for most datasets; for complete results of resampling, including the opposite direction effects, see https://doi.org/10.5281/zenodo.4744720.

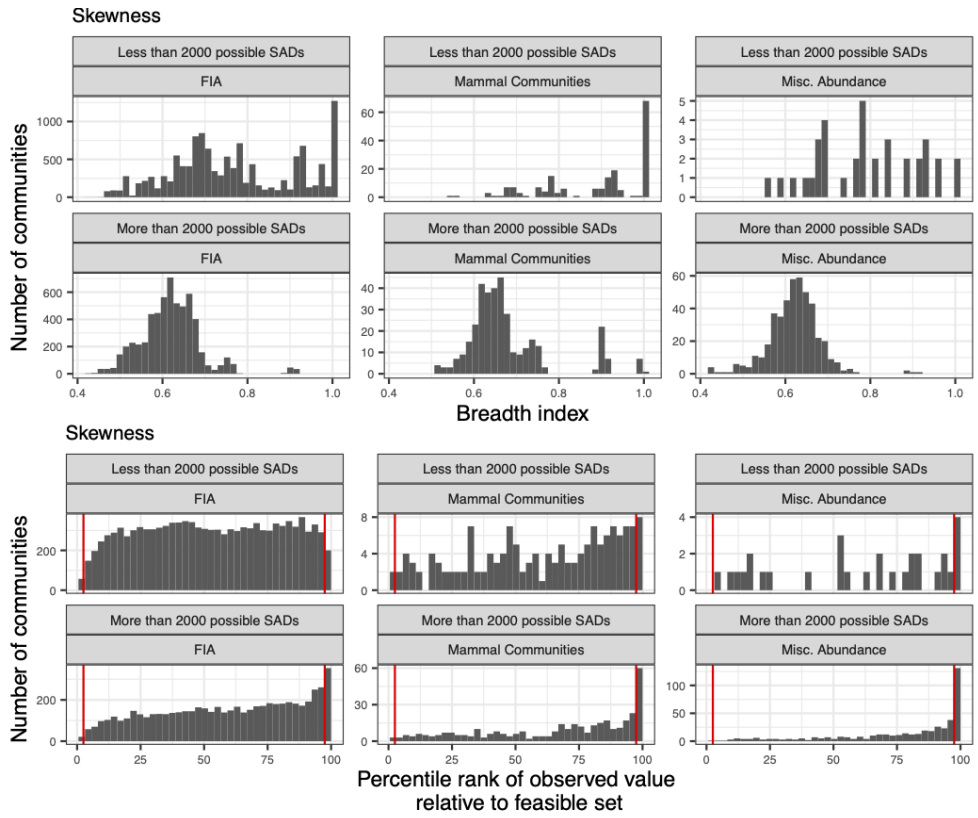

Figure 4-6. Very small communities (e.g. those with fewer than 2000 possible SADs in the feasible set; upper rows) exhibit more variable, broadly-defined statistical baselines (top) and less consistently extreme observed values relative to their feasible sets (bottom). 2000 possible SADs is used as a cutoff because it allows for a comparison using a substantial number of communities from the FIA and two other datasets. Of these datasets, the FIA is the most dominated by very small communities (68% of FIA sites have fewer than 2000 possible SADs, compared to 34% for the Mammal Community and 7% for the Miscellaneous Abundance databases). Results shown are for skewness; for complete results see https://doi.org/10.5281/zenodo.4744720.

4.6 Tables for Chapter 4

Table 4-1. Proportions of extreme values for percentile scores for observed SADs compared to samples from the feasible set. For dissimilarity, this is the proportion of percentile scores >95; by chance, 5% of scores should be in this extreme. For all other metrics, this is the proportion <2.5 or >97.5; by chance 2.5% of scores should be in either extreme. *n* refers to the number of communities included for each dataset for each metric. The proportions shown are for the directions of effects observed for most datasets; for the opposite-direction effects, see https://doi.org/10.5281/zenodo.4744720.

Dataset	High dissimilarity	High proportion of rare species	High skew	Low Simpson	Low Shannon
Breeding Bird Survey	23%; n = 2773	4.5%; n = 2773	9%; n = 2773	21%; n = 2773	23%; n = 2773
FIA	7.2%; n = 18447	1.4%; n = 17410	2.8%; n = 17410	5.8%; n = 17410	5.5%; n = 17410
Gentry	34%; n = 224	0.9%; n = 223	11%; n = 223	9.9%; n = 223	7.6%; n = 223
Mammal Communities	32%; n = 552	13%; n = 511	12%; n = 505	28%; n = 511	30%; n = 511
Misc. Abundance	59%; n = 494	27%; n = 486	27%; n = 484	53%; n = 486	56%; n = 486

CHAPTER 5
CONCLUSION

This dissertation traverses the range of views afforded by a macroecological lens on community structure and dynamics, spanning three distinct organizational and spatial scales and contrasting methods of scientific inquiry. Chapter 2 focuses on the link between species interactions and community properties in a single system, using a long-running manipulative experiment to disentangle nuanced dynamics of compensation and competition. Chapter 3 uses modern advances in computational infrastructure and data-intensive ecology to perform an observational, data-driven synthesis of long-term biodiversity dynamics for bird communities across the continent of North America. Finally, chapter 4 steps beyond the traditional scope of ecology to apply theoretical approaches derived from statistical mechanics to understand the significance of ecological ”laws”, using data from communities across the globe and tree of life.

Methodologically, these chapters leverage traditional methods in community ecology - community surveys, manipulative exclosure experiments, population trend monitoring - and combine them with the tools of modern data science to achieve large-scale synthesis. Building from the empirically-grounded Chapter 2, Chapters 3 and 4 use massive compilations of ecological data, and high-performance computational methods, to characterize general trends and phenomena in ecological communities at continental and global scales. These analyses are made possible by a rich and robust ecosystem of openly available and community-maintained ecological datasets and software packages, and have themselves generated R packages implementing new algorithms and data-generating pipelines to facilitate further advances in macroecology and biodiversity science. These methodological synergies are a promising path forward for the development of macroecology and community ecology in an increasingly data-driven world.

At a conceptual level, Chapters 2 and 3 illustrate how manipulative field experiments can spark questions that inspire larger-scale observational synthesis. The long-term dynamics of energy use, community-wide biomass, and community structure of the rodent community that form the focus of Chapter 2 parallel the interrelated long-term trends in total individual abundance, biomass, and energy use that are the subject of Chapter 3. The deep natural history basis of Chapter 2 affords mechanistic insight into the community and population-level processes

that modulate community-level properties in a specific community, but cannot establish the generality of these phenomena extending beyond this system. As a complement to this system-specific work, Chapter 3 explores continent-wide trends in how individual abundance, biomass, and energy use fluctuate in bird communities across North America - but at the sacrifice of mechanistic insight into the processes driving these fluctuations. Chapter 4 demonstrates how community ecology stands to benefit from, and contribute to, conceptual developments drawn from the broad and rich fabric of complex systems studies. In applying the concept of a ”statistical baseline” to understand the ecological species abundance distribution, Chapter 4 treats ecological communities as analogous to the complex systems more usually studied under the purview of physics or statistical mechanics. However, ecological systems present statistical challenges that are not common in these more traditionally ”complex” disciplines. By using novel sampling algorithms, and engaging directly with the statistical irregularities inherent to ecological communities, Chapter 4 begins to address fundamental questions about the nature and inferential power of emergent complex phenomena not restricted to ecology.

Separately, the vignettes presented here illustrate the value, and the limitations, of distinct approaches and scales of inquiry in community ecology. Combined, they demonstrate the unique conceptual and methodological insights gleaned through an integrative macroecological approach. Taken as a unit, this dissertation embodies a macroecology that is empirically grounded, intellectually adventurous, and poised to embrace the breadth and depth of analysis made possible by a cross-disciplinary and data-driven approach to biodiversity science in the 21st century.

APPENDIX A
SUPPLEMENTAL RESULTS AND ANALYSES FOR CHAPTER 2

A.1 Plot-level analysis

A.1.1 Explanation

In order to calculate energetic compensation and the total energy ratio, we require an estimate for the baseline values of total energy use, kangaroo rat energy use, and small granivore energy use on control plots. Estimating these baselines requires aggregating over between-plot variability among the control plots. For consistency, in the main analysis, we also aggregate across the exclosure plots and focus on treatment-level means throughout. Here, we explore the effect of between-plot variability on our analyses, to the extent possible. We used treatment-level means across control plots to calculate energetic compensation and the total energy ratio, but calculated these quantities separately for each exclosure plot, and conducted analyses including a random effect of plot. We also conducted analyses of Dipodomys and C. baileyi proportional energy use using plot-level data, again including plot as a random effect. Results were qualitatively the same as using treatment-level means.

A.1.2 Compensation

We fit linear mixed-effects models (using the *lme* function in the R package *nlme*; [86]) of the form $compensation = timeperiod$ with a random effect of plot and temporal autocorrelation structure to account for autocorrelation between monthly census periods within each time period. We compared these to models without the autocorrelation structure, without the random effect, and without the term for time period. The best-fitting model included terms for time period, random effect of plot, and autocorrelation.

A.1.3 Total energy use

As for compensation, we fit linear mixed-effects models fitting *total energy ratio* = *time period* with a random effect of plot and a temporal autocorrelation term to account for autocorrelation between monthly census periods within each timeperiod. We compared these to models without the autocorrelation term, without the random effect, and without the term for time period. The best-fitting model included terms for time period, random effect of plot, and autocorrelation.

A.1.4 *Dipodomys* proportional energy use

To compare proportional energy use across time periods, we used binomial generalized linear mixed models (using the glmer function in the R package *lme4*; Bates (2015)), which allowed us to include a random effect of plot.

For *Dipodomys* proportional energy use, we compared models with and without the random effect of plot and with and without a term for timeperiod. The best-fitting model included terms for timeperiod and a random effect of plot.

A.1.5 *C. baileyi* proportional energy use

As for kangaroo rat proportional energy use, we used a binomial generalized linear mixed effects model to compare *C. baileyi* proportional energy use across time periods. Because *C. baileyi* occurs on both control and exclosure plots, we investigated whether the dynamics of *C. baileyi*'s proportional energy use differed between treatment types. We compared models incorporating separate slopes, separate intercepts, or no terms for treatment modulating the change in *C. baileyi* proportional energy use across time periods, i.e. comparing the full set of models:

- *c baileyi proportional energy use = timeperiod + treatment + timeperiod:treatment*

-c baileyi proportional energy use = 1

- *c baileyi proportional energy use = timeperiod*

We also tested a null (intercept-only) model of no change across time periods:

- *c baileyi proportional energy use = 1*

We compared all of these models with and without a random effect of plot. We found that the best-fitting model incorporated a random effect of plot, and fixed effects for time period and for treatment, but no interaction between them (*c baileyi proportional energy use = 1*). We therefore proceeded with this model.

A.1.6 Tables

Table A-1. Plot-level: Model comparison for compensation.

Model specification	AIC
intercept + timeperiod + plot (random effect) + autocorrelation	1360.207
intercept + timeperiod + plot (random effect)	1680.916
intercept + timeperiod + autocorrelation	1409.830
intercept + plot (random effect) + autocorrelation	1408.362
intercept + plot (random effect)	1879.126
intercept	2036.371

Table A-2. Plot-level: Coefficients from linear mixed-effects model for compensation.

	Value	Std.Error	DF	t-value	p-value
(Intercept)	0.3451282	0.1048354	1362	3.292096	0.0010199
oera.L	0.0653090	0.0373313	1362	1.749446	0.0804392
oera.Q	-0.2845830	0.0341063	1362	-8.343990	0.0000000

Table A-3. Plot-level: Estimates from linear mixed-effects model for compensation.

Timeperiod	emmean	SE	df	lower.CL	upper.CL
1988-1997	0.1827673	0.1091842	3	-0.1647055	0.5302400
1997-2010	0.5774892	0.1078860	3	0.2341478	0.9208306
2010-2020	0.2751282	0.1093969	3	-0.0730215	0.6232779

Table A-4. Plot-level: Contrasts from linear mixed-effects model for compensation.

Comparison	estimate	SE	df	t.ratio	p.value
1988-1997 - 1997-2010	-0.3947220	0.0491845	1362	-8.025330	0.0000
1988-1997 - 2010-2020	-0.0923609	0.0527944	1362	-1.749446	0.1873
1997-2010 - 2010-2020	0.3023610	0.0496411	1362	6.090948	0.0000

Table A-5. Plot-level: Model comparison for total energy use.

Model specification	AIC
intercept + timeperiod + plot (random effect) + autocorrelation	474.8558
intercept + timeperiod + plot (random effect)	924.1830
intercept + timeperiod + autocorrelation	507.7842
intercept + plot (random effect) + autocorrelation	543.5425
intercept + plot (random effect)	1266.2097
intercept	1382.7469

Table A-6. Plot-level: Coefficients from linear mixed-effects model for total energy ratio.

	Value	Std.Error	DF	t-value	p-value
(Intercept)	0.5018200	0.0709701	1362	7.070865	0.0e+00
oera.L	0.1454309	0.0301324	1362	4.826392	1.5e-06
oera.Q	-0.2545852	0.0273660	1362	-9.302977	0.0e+00

Table A-7. Plot-level: Estimates from linear mixed-effects model for total energy ratio.

Timeperiod	emmean	SE	df	lower.CL	upper.CL
1988-1997	0.2950508	0.0751321	3	0.0559470	0.5341547
1997-2010	0.7096879	0.0738511	3	0.4746606	0.9447151
2010-2020	0.5007212	0.0752881	3	0.2611207	0.7403216

Table A-8. Plot-level: Contrasts from linear mixed-effects model for total energy ratio.

Comparison	estimate	SE	df	t.ratio	p.value
1988-1997 - 1997-2010	-0.4146370	0.0395736	1362	-10.477622	0.0e+00
1988-1997 - 2010-2020	-0.2056703	0.0426137	1362	-4.826392	4.6e-06
1997-2010 - 2010-2020	0.2089667	0.0398571	1362	5.242901	5.0e-07

Table A-9. Plot-level: Model comparison for kangaroo rat proportional energy use.

Model specification	AIC
intercept + timeperiod + plot (random effect)	1040.861
intercept + plot (random effect)	1162.470
intercept + timeperiod	1108.490
intercept	1208.081

Table A-10. Plot-level: Coefficients from GLMER on kangaroo rat energy use.

	Estimate	Std. Error	z.value	$Pr(>\|z\|)$
(Intercept)	2.181163	0.1305753	16.704251	0
oera.L	-1.946096	0.2664545	-7.303670	0
oera.Q	1.124620	0.1769225	6.356572	0

Table A-11. Plot-level: Estimates from GLMER on kangaroo rat energy use.

Timeperiod	prob	SE	df	asymp.LCL	asymp.UCL
1988-1997	0.9823009	0.0062020	Inf	0.9701452	0.9944566
1997-2010	0.7795273	0.0183934	Inf	0.7434769	0.8155777
2010-2020	0.7797464	0.0208516	Inf	0.7388780	0.8206149

Table A-12. Plot-level: Contrasts from GLMER on kangaroo rat energy use.

Comparison	estmimate	SE	df	z.ratio	p.value
1988-1997 - 1997-2010	0.2027736	0.0194108	Inf	10.4464200	0
1988-1997 - 2010-2020	0.2025545	0.0217545	Inf	9.3109407	0
1997-2010 - 2010-2020	-0.0002191	0.0278048	Inf	-0.0078811	1

Table A-13. Plot-level: Model comparison for *C. baileyi* proportional energy use.

Model specification	AIC
intercept + timeperiod + treatment + timeperiod:treatment + plot (random effect)	1021.318
intercept + timeperiod + treatment + plot (random effect)	1020.263
intercept + timeperiod + plot (random effect)	1042.758
intercept + plot (random effect)	1321.149
intercept + timeperiod + treatment + timeperiod:treatment	1166.653
intercept + timeperiod + treatment	1162.901
intercept + timeperiod	1869.097
intercept	2036.489

Table A-14. Plot-level: Coefficients from GLMER on *C. baileyi* energy use.

	Estimate	Std. Error	z.value	$Pr(>\|z\|)$
(Intercept)	-2.443643	0.2067789	-11.81766	0
oera.L	-1.866286	0.1530068	-12.19740	0
oera.Q	3.265183	0.2913472	11.20719	0

Table A-15. Plot-level: Estimates from GLMER on *C. baileyi* energy use.

Timeperiod	Treatment	prob	SE	df	asymp.LCL	asymp.UCL
1997-2010	Control	0.0312856	0.0116044	Inf	0.0085414	0.0540297
1997-2010	Exclosure	0.7658194	0.0392864	Inf	0.6888195	0.8428193
2010-2020	Control	0.0023009	0.0008486	Inf	0.0006378	0.0039641
2010-2020	Exclosure	0.1893142	0.0364430	Inf	0.1178872	0.2607412

Table A-16. Plot-level: Contrasts from GLMER on *C. baileyi* energy use.

Comparison	Treatment	estimate	SE	df	z.ratio	p.value
1997-2010 - 2010-2020	Control	2.639326	0.2163843	Inf	12.1974	0
1997-2010 - 2010-2020	Exclosure	2.639326	0.2163843	Inf	12.1974	0

A.2 Full model results

A.2.1 Compensation

We fit a generalized least squares (of the form $compensation = timeperiod$; note that "timeperiod" is coded as "oera" throughout) using the *gls* function from the R package *nlme* [86]. Because values from monthly censuses within each time period are subject to temporal autocorrelation, we included a continuous autoregressive temporal autocorrelation structure of order 1 (using the *CORCAR*1 function). We compared this model to models fit without the autocorrelation structure and without the time period term using AIC. The model with both the time period term and the autocorrelation structure was the best-fitting model via AIC, and we used this model to calculate estimates and contrasts using the package *emmeans* [63].

A.2.2 Total energy use ratio

As for compensation, we fit a generalized least squares of the form *total energy ratio* = *timeperiod*, accounting for temporal autocorrelation between monthly censuses within each time period using a continuous autoregressive autocorrelation structure of order 1. We compared this model to models fit without the timeperiod term and/or autocorrelation structure, and found the full (timeperiod plus autocorrelation) model had the best performance via AIC. We used this model for estimates and contrasts.

A.2.3 *Dipodomys* proportional energy use

Proportional energy use is bounded 0-1 and cannot be fit with generalized least squares. We therefore used a binomial generalized linear model of the form *Dipodomys proportional energy use = timeperiod*. We compared a model fit with a timeperiod term to an intercept-only (null) model using AIC, and found the timeperiod term improved model fit. We used this model for estimates and contrasts.

Note that we were unable to incorporate temporal autocorrelation into generalized linear models, and we prioritized fitting models of the appropirate family over accounting for autocorrelation. Due to the pronounced differences between time periods for these variables, we were comfortable proceeding without explicitly accounting for autocorrelation.

A.2.4 *C. baileyi* proportional energy use

As for kangaroo rat proportional energy use, we used a binomial generalized linear model to compare *C. baileyi* proportional energy use across time periods. Because *C. baileyi* occurs on both control and exclosure plots, we investigated whether the dynamics of *C. baileyi*'s proportional energy use differed between treatment types. We compared models incorporating separate slopes, separate intercepts, or no terms for treatment modulating the change in *C. baileyi* proportional energy use across time periods, i.e. comparing the full set of models:

- *c baileyi proportional energy use = timeperiod + treatment + timeperiod:treatment*

- *c baileyi proportional energy use = timeperiod + treatment*

- *c baileyi proportional energy use = timeperiod* We also tested a null (intercept-only) model of no change across time periods:

- *c baileyi proportional energy use = 1*

We found that the best-fitting model incorporated effects for time period and for treatment, but no interaction between them (*c baileyi proportional energy use = timeperiod + treatment*). We therefore proceeded with this model.

A.2.5 Tables

Table A-17. Model comparison for compensation.

Model specification	AIC
intercept + timeperiod + autocorrelation	69.85023
intercept + autocorrelation	84.74902
intercept + timeperiod	157.09726
intercept	252.74534

Table A-18. Coefficients from GLS model for compensation.

	Value	Std.Error	t-value	p-value
(Intercept)	0.3450313	0.0294996	11.696141	0.0000000
oera.L	0.0647933	0.0524103	1.236269	0.2172146
oera.Q	-0.2833553	0.0477359	-5.935890	0.0000000

Table A-19. Estimates from GLS for compensation.

Timeperiod	emmean	SE	df	lower.CL	upper.CL
1988-1997	0.1835362	0.0520378	44.11081	0.0786683	0.2884041
1997-2010	0.5763899	0.0462641	47.37851	0.4833383	0.6694416
2010-2020	0.2751677	0.0528010	46.75897	0.1689314	0.3814041

Table A-20. Contrasts from GLS for compensation.

Comparison	estimate	SE	df	t.ratio	p.value
1988-1997 - 1997-2010	-0.3928537	0.0689413	47.89422	-5.698378	0.0000
1988-1997 - 2010-2020	-0.0916315	0.0741194	45.51740	-1.236269	0.4383
1997-2010 - 2010-2020	0.3012222	0.0694989	49.52957	4.334200	0.0002

Table A-21. Model comparison for total energy use.

Model specification	AIC
intercept + timeperiod + autocorrelation	-132.92138
intercept + autocorrelation	-118.15000
intercept + timeperiod	13.29396
intercept	156.85988

Table A-22. Coefficients from GLS for total energy ratio.

	Value	Std.Error	t-value	p-value
(Intercept)	0.5016731	0.0271176	18.499880	0.0000000
oera.L	0.1413504	0.0477646	2.959316	0.0033001
oera.Q	-0.2503659	0.0429312	-5.831790	0.0000000

Table A-23. Estimates from GLS for total energy ratio.

Timeperiod	emmean	SE	df	lower.CL	upper.CL
1988-1997	0.2995118	0.0475806	36.19943	0.2030323	0.3959913
1997-2010	0.7060960	0.0419773	38.51943	0.6211550	0.7910369
2010-2020	0.4994115	0.0480066	37.62774	0.4021956	0.5966274

Table A-24. Contrasts from GLS for total energy ratio.

Comparison	estimate	SE	df	t.ratio	p.value
1988-1997 - 1997-2010	-0.4065842	0.0623398	40.51631	-6.522060	0.0000
1988-1997 - 2010-2020	-0.1998997	0.0675493	37.12310	-2.959316	0.0144
1997-2010 - 2010-2020	0.2066845	0.0626456	41.44768	3.299267	0.0056

Table A-25. Model comparison for kangaroo rat proportional energy use.

Model specification	AIC
intercept + timeperiod	258.3581
intercept	280.8497

Table A-26. Coefficients from GLM on kangaroo rat energy use.

	Estimate	Std. Error	z.value	$Pr(>\|z\|)$
(Intercept)	1.4032480	0.1503201	9.335068	0.0000000
oera.L	-1.1000833	0.2871738	-3.830723	0.0001278
oera.Q	0.5855493	0.2304516	2.540878	0.0110574

Table A-27. Estimates from GLM on kangaroo rat energy use.

Timeperiod	prob	SE	df	asymp.LCL	asymp.UCL
1988-1997	0.9183528	0.0256462	Inf	0.8680872	0.9686183
1997-2010	0.7160901	0.0398537	Inf	0.6379782	0.7942020
2010-2020	0.7035835	0.0456677	Inf	0.6140765	0.7930905

Table A-28. Contrasts from GLM on kangaroo rat energy use.

Comparison	estimate	SE	df	z.ratio	p.value
1988-1997 - 1997-2010	1.4950249	0.3942281	Inf	3.7922836	0.0004
1988-1997 - 2010-2020	1.5557527	0.4061251	Inf	3.8307227	0.0004
1997-2010 - 2010-2020	0.0607279	0.2938992	Inf	0.2066282	0.9767

Table A-29. Model comparison for *C. baileyi* proportional energy use.

Model specification	AIC
intercept + timeperiod + treatment + timeperiod:treatment	237.7643
intercept + timeperiod + treatment	231.0963
intercept + timeperiod	460.8477
intercept	541.3799

Table A-30. Coefficients from GLM on *C. baileyi* energy use.

	Estimate	Std. Error	z.value	$Pr(>\|z\|)$
(Intercept)	-1.574028	0.1670168	-9.424368	0
oera.L	-1.409273	0.2010398	-7.009921	0
oplottype.L	2.184896	0.2267112	9.637355	0

Table A-31. Estimates from GLM on *C. baileyi* energy use.

Timeperiod	Treatment	prob	SE	df	asymp.LCL	asymp.UCL
1997-2010	Control	0.1069314	0.0258894	Inf	0.0561890	0.1576737
1997-2010	Exclosure	0.7246076	0.0385129	Inf	0.6491236	0.8000915
2010-2020	Control	0.0160560	0.0058224	Inf	0.0046444	0.0274676
2010-2020	Exclosure	0.2639419	0.0428458	Inf	0.1799657	0.3479181

Table A-32. Contrasts from GLM on *C. baileyi* energy use.

Comparison	Treatment	estimate	SE	df	z.ratio	p.value
1997-2010 - 2010-2020	Control	1.993013	0.2843132	Inf	7.009921	0
1997-2010 - 2010-2020	Exclosure	1.993013	0.2843132	Inf	7.009921	0

A.3 Biomass analysis

A.3.1 Compensation

We fit a generalized least squares (of the form $compensation = timeperiod$; note that "timeperiod" is coded as "oera" throughout) using the *gls* function from the R package *nlme* [86]. Because values from monthly censuses within each time period are subject to temporal autocorrelation, we included a continuous autoregressive temporal autocorrelation structure of order 1 (using the *CORCAR*1 function). We compared this model to models fit without the

autocorrelation structure and without the time period term using AIC. The model with both the time period term and the autocorrelation structure was the best-fitting model via AIC, and we used this model to calculate estimates and contrasts using the package *emmeans* [63].

A.3.2 Total biomass ratio

As for compensation, we fit a generalized least squares of the form *total energy ratio* = *timeperiod*, accounting for temporal autocorrelation between monthly censuses within each time period using a continuous autoregressive autocorrelation structure of order 1. We compared this model to models fit without the timeperiod term and/or autocorrelation structure, and found the full (timeperiod plus autocorrelation) model had the best performance via AIC. We used this model for estimates and contrasts.

A.3.3 *Dipodomys* proportional biomass

Proportional biomass is bounded 0-1 and cannot be fit with generalized least squares. We therefore used a binomial generalized linear model of the form *Dipodomys proportional biomass* = *timeperiod*. We compared a model fit with a timeperiod term to an intercept-only (null) model using AIC, and found the timeperiod term improved model fit. We used this model for estimates and contrasts.

Note that we were unable to incorporate temporal autocorrelation into generalized linear models, and we prioritized fitting models of the appropirate family over accounting for autocorrelation. Due to the pronounced differences between time periods for these variables, we were comfortable proceeding without explicitly accounting for autocorrelation.

A.3.4 *C. baileyi* proportional biomass

As for kangaroo rat proportional biomass, we used a binomial generalized linear model to compare *C. baileyi* proportional biomass across time periods. Because *C. baileyi* occurs on both control and exclosure plots, we investigated whether the dynamics of *C. baileyi*'s proportional biomass differed between treatment types. We compared models incorporating separate slopes, separate intercepts, or no terms for treatment modulating the change in *C. baileyi* proportional biomass across time periods, i.e. comparing the full set of models:

- *c baileyi proportional biomass = timeperiod + treatment + timeperiod:treatment*

- *c baileyi proportional biomass = timeperiod + treatment*

- *c baileyi proportional biomass = timeperiod* We also tested a null (intercept-only) model of no change across time periods:

- *c baileyi proportional biomass = 1*

We found that the best-fitting model incorporated effects for time period and for treatment, but no interaction between them (*c baileyi proportional biomass = timeperiod + treatment*). We therefore proceeded with this model.

A.3.5 Tables

Table A-33. Model comparison for compensation.

Model specification	AIC
intercept + timeperiod + autocorrelation	-17.623354
intercept + autocorrelation	-3.297103
intercept + timeperiod	92.184205
intercept	207.804481

Table A-34. Coefficients from GLS model for compensation.

	Value	Std.Error	t-value	p-value
(Intercept)	0.3081443	0.0290539	10.605950	0.0000000
oera.L	0.0711412	0.0514131	1.383719	0.1673549
oera.Q	-0.2799121	0.0465252	-6.016352	0.000000

Table A-35. Estimates from GLS for compensation.

Timeperiod	emmean	SE	df	lower.CL	upper.CL
1988-1997	0.1435663	0.0511419	39.28312	0.0401458	0.2469867
1997-2010	0.5366915	0.0452745	41.91562	0.4453185	0.6280646
2010-2020	0.2441751	0.0517205	41.17937	0.1397373	0.3486130

Table A-36. Contrasts from GLS for compensation.

Comparison	estimate	SE	df	t.ratio	p.value
1988-1997 - 1997-2010	-0.3931253	0.0673811	43.22895	-5.834358	0.0000
1988-1997 - 2010-2020	-0.1006089	0.0727090	40.36882	-1.383719	0.3588
1997-2010 - 2010-2020	0.2925164	0.0678003	44.43055	4.314383	0.0003

Table A-37. Model comparison for total biomass.

Model specification	AIC
intercept + timeperiod + autocorrelation	-176.57761
intercept + autocorrelation	-162.61339
intercept + timeperiod	-15.98438
intercept	146.61442

Table A-38. Coefficients from GLS for total biomass ratio.

	Value	Std.Error	t-value	p-value
(Intercept)	0.4553971	0.0272418	16.716827	0.0000000
oera.L	0.1454493	0.0477989	3.042941	0.0025257
oera.Q	-0.2531409	0.0427343	-5.923594	0.0000000

Table A-39. Estimates from GLS for total biomass ratio.

Timeperiod	emmean	SE	df	lower.CL	upper.CL
1988-1997	0.2492046	0.0476584	33.82432	0.1523326	0.3460765
1997-2010	0.6620857	0.0419515	35.98516	0.5770030	0.7471684
2010-2020	0.4549009	0.0480215	34.98703	0.3574107	0.5523911

Table A-40. Contrasts from GLS for total biomass ratio.

Comparison	estimate	SE	df	t.ratio	p.value
1988-1997 - 1997-2010	-0.4128811	0.0621739	38.42746	-6.640747	0.0000
1988-1997 - 2010-2020	-0.2056963	0.0675979	34.67694	-3.042941	0.0121
1997-2010 - 2010-2020	0.2071848	0.0624325	39.20390	3.318542	0.0054

Table A-41. Model comparison for kangaroo rat proportional biomass.

Model specification	AIC
intercept + timeperiod	215.2069
intercept	227.9608

Table A-42. Coefficients from GLM on kangaroo rat biomass.

	Estimate	Std. Error	z.value	$Pr(>\|z\|)$
(Intercept)	1.6149566	0.1644937	9.817741	0.0000000
oera.L	-1.1672395	0.3180813	-3.669626	0.0002429
oera.Q	0.6619048	0.2473324	2.676175	0.0074468

Table A-43. Estimates from GLM on kangaroo rat biomass.

Timeperiod	prob	SE	df	asymp.LCL	asymp.UCL
1988-1997	0.9376458	0.0226460	Inf	0.8932605	0.9820310
1997-2010	0.7454543	0.0385025	Inf	0.6699909	0.8209177
2010-2020	0.7426552	0.0437171	Inf	0.6569713	0.8283392

Table A-44. Contrasts from GLM on kangaroo rat biomass.

Comparison	estimate	SE	df	z.ratio	p.value
1988-1997 - 1997-2010	1.6360275	0.4372643	Inf	3.741508	0.0005
1988-1997 - 2010-2020	1.6507259	0.4498349	Inf	3.669626	0.0007
1997-2010 - 2010-2020	0.0146984	0.3057707	Inf	0.048070	0.9987

Table A-45. Model comparison for *C. baileyi* proportional biomass.

Model specification	AIC
intercept + timeperiod + treatment + timeperiod:treatment	237.6847
intercept + timeperiod + treatment	231.2374
intercept + timeperiod	466.4937
intercept + treatment	346.2154
intercept	543.7811

Table A-46. Coefficients from GLM on *C. baileyi* biomass.

	Estimate	Std. Error	z.value	$Pr(>\|z\|)$
(Intercept)	-1.538798	0.1671239	-9.207525	0
oera.L	-1.403286	0.2006948	-6.992140	0
oplottype.L	2.270657	0.2298594	9.878462	0

Table A-47. Estimates from GLM on *C. baileyi* biomass.

Timeperiod	Treatment	prob	SE	df	asymp.LCL	asymp.UCL
1997-2010	Control	0.1041331	0.0255800	Inf	0.0539971	0.1542691
1997-2010	Exclosure	0.7425132	0.0376727	Inf	0.6686761	0.8163504
2010-2020	Control	0.0157248	0.0057341	Inf	0.0044861	0.0269634
2010-2020	Exclosure	0.2838438	0.0439192	Inf	0.1977637	0.3699240

Table A-48. Contrasts from GLM on *C. baileyi* biomass.

Comparison	Treatment	estimate	SE	df	z.ratio	p.value
1997-2010 - 2010-2020	Control	1.984546	0.2838253	Inf	6.99214	0
1997-2010 - 2010-2020	Exclosure	1.984546	0.2838253	Inf	6.99214	0

A.4 Covariates of rodent community change

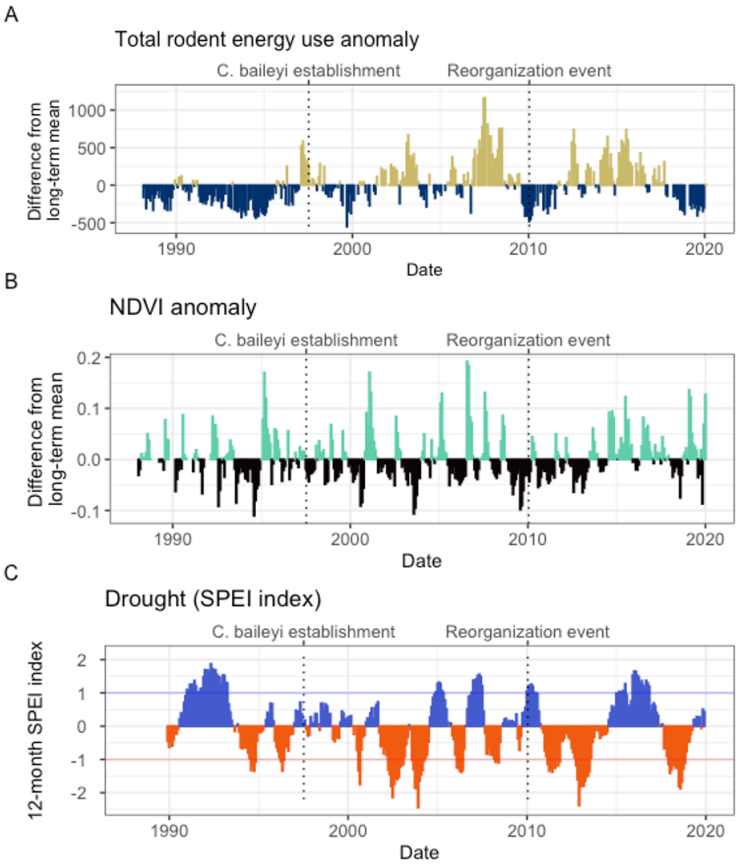

Figure A-1. Changes in overall community energy use (A), NDVI (B), and local climate (C) surrounding the 2010 shift in rodent community composition. As documented in [14], the 2010 transition followed a period of low abundance community-wide (A) and low plant productivity (B). Since 2010, the site has experienced two periods of drought (C) interspersed with an unusually wet period. Total rodent energy use (A) is calculated as the total energy use of all granviores on control plots ($Etot_C$) in each census period. The anomaly (shown) is calculated as the difference between the total energy use in each census period and the long-term mean of total energy use. Vertical dashed lines mark the dates of major transitions in the rodent community. NDVI anomaly (B) is calculated as the difference between monthly NDVI and the long-term mean for that month. NDVI data were obtained from Landsat 5, 7, and 8 using the *ndvi* function in the R package *portalr* [68, 109, 15]. Drought (C) was calculated using a 12-month Standardized Precipitation Evapotranspiraiton index (SPEI) for all months from 1989-2020, using the Thornthwaite method to estimate potential evapotranspiration (using the R package *SPEI*; [3, 99, 11]). Values greater than 0 (blue) indicate wetter than average conditions, and values less than 0 (red) indicate drier conditions. Values between -1 and 1 (horizontal lines) are considered within normal variability for a system, while values ¡ -1 constitute drought [99].

APPENDIX B
SUPPLEMENTAL FIGURES AND TABLES FOR CHAPTER 3

B.1 Results for routes with complete temporal sampling

Figures and tables from the main analysis, restricted to 199 routes with perfect temporal coverage (i.e. no missing time steps). All results are qualitatively the same as for the main analysis (739 routes, with a minimum of 27 of 30 time steps sampled for each route).

B.1.1 Figures

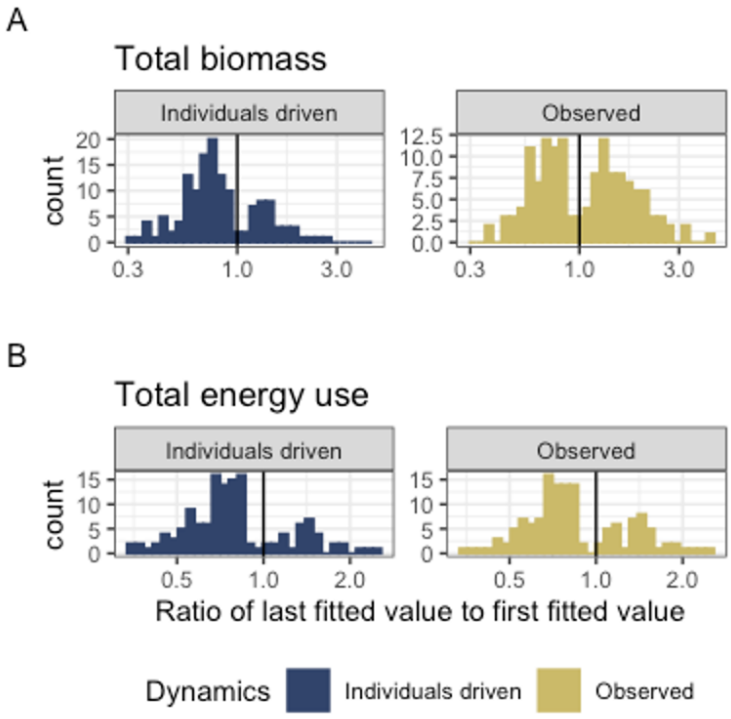

Figure B-1. Histograms showing the direction and magnitude of long-term trends for the individuals-driven (null-model; left) and observed (right) changes in biomass (A) and energy use (B), for communities with a significant slope and/or interaction term (for biomass, 141/199 routes; for energy use, 137/199 routes; Table B-1). Change is summarized as the ratio of the fitted value for the last year in the time series to the fitted value for the first year in the timeseries from the best-fitting model for that community. Values greater than 1 (vertical black line) indicate increases in total energy or biomass over time, and less than 1 indicate decreases. The individuals-driven dynamics (left) reflect the trends fit for the null model, while the observed dynamics (right) reflect trends incorporating both change in total abundance and change in the size structure over time. For communities best-described by syndromes of "coupled trends" or "no directional change", the "individuals-driven" and "observed" ratios will be the same; for communities with "decoupled trends", there will be different ratios for or "individuals-driven" and "observed" dynamics. Among routes with temporal trends ("coupled trends" or "decoupled trends"), there are qualitatively different continental-wide patterns in individuals-driven and observed dynamics for total biomass and total energy use. 76% of trends in individuals-driven (null model) dynamics for energy use are decreasing, and 72% for biomass (Table B-2). For biomass, observed dynamics are balanced evenly between increases (50% of routes) and decreases (50%) - indicating that changes in the size structure produce qualitatively different long-term trends for biomass than would be expected given abundance changes alone. However, trends for energy use (which scales nonlinearly with biomass) are dominated by decreases (69% of routes), more closely mirroring the trends expected given changes in individual abundance alone.

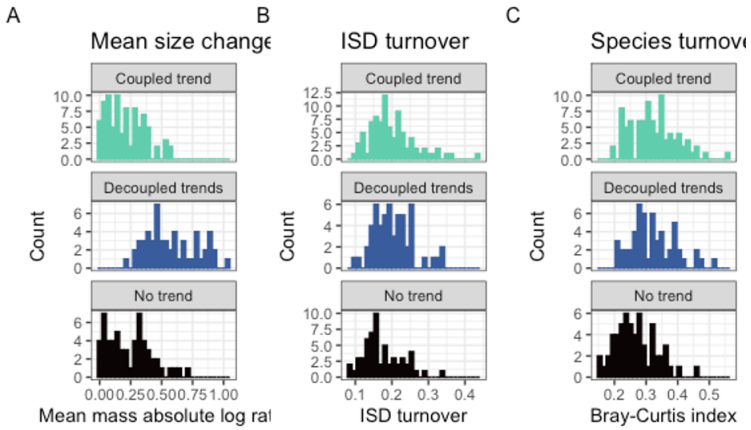

Figure B-2. Histograms of (A) change in mean body size from the first to the last five years of monitoring, (B) overall change in the size structure, and (C) change in species composition for routes whose dynamics for total biomass were best-described using no temporal trend (bottom row; intercept-only model), separate trends for observed and individuals-driven dynamics (middle row), or the same trend for observed and individuals-driven dynamics (top row). Change in mean body size (A) is calculated as the ratio of the mean body size of all individuals observed in the last 5 years of the timeseries relative to the mean body size of all individuals observed in the first 5 years. Overall change in the ISD (B) is calculated as the degree of turnover between the ISDs for the first and last five years of the timeseries (see text). Change in species composition (C) is Bray-Curtis dissimilarity comparing species composition in the first five years to the last five years.

B.1.2 Tables

Table B-1. The number and proportion of routes whose dynamics for total biomass and total energy use are best described by the following syndromes: no directional change (intercept-only model, *biomass = 1* or *energy use = 1*); a coupled trend (*biomass = year* or *energy use = year*); or a model with decoupled temporal trends for observed and individuals-driven dynamics (*biomass = year * dynamics* or *energy use = year * dynamics*, where *dynamics* refers to observed or null model, individuals-driven dynamics).

Currency	Selected model	Number of routes	Proportion of routes
Total biomass	Intercept-only	58	0.29
Total biomass	Trend, not decoupled	86	0.43
Total biomass	Decoupled trend	55	0.28
Total energy use	Intercept-only	62	0.31
Total energy use	Trend, not decoupled	115	0.58
Total energy use	Decoupled trend	22	0.11

Table B-2. The proportion of trends that are increasing (specifically, for which the ratio of the last fitted value to the first fitted value ¿ 1) for individuals-driven and observed dynamics, for routes exhibiting temporal trends ("coupled trends" or "decoupled trends") in total biomass and total energy use. Trends that are not increasing are decreasing.

Currency	Proportion of increasing individuals-driven trends	Proportion of increasing observed trends	Number of routes with temporal trends
Total biomass	0.28	0.50	141
Total energy use	0.24	0.31	137

Table B-3. ANOVA table comparing ordinary linear models of the form *absolute log ratio = syndrome* and *absolute log ratio = 1*.

Res.Df	RSS	Df	Sum of Sq	F	$Pr(>F)$
196	5.993024	NA	NA	NA	NA
198	11.105203	-2	-5.11218	83.59613	0

Table B-4. Estimates (calculated using *emmeans* [63]) for the mean absolute log ratio of mean mass for routes whose dynamics for biomass were best-described by different syndromes of change.

categorical fit	emmean	SE	df	lower.CL	upper.CL
Coupled trend	0.2084997	0.0188558	196	0.1713133	0.2456861
Decoupled trends	0.5779023	0.0235784	196	0.5314024	0.6244021
No trend	0.2385438	0.0229605	196	0.1932625	0.2838251

Table B-5. Contrasts for absolute log ratio of mean mass, calculated using *emmeans* [63].

contrast	estimate	SE	df	t.ratio	p.value
Coupled trend - Decoupled trends	-0.3694026	0.0301908	196	-12.235620	0.0000000
Coupled trend - No trend	-0.0300441	0.0297107	196	-1.011221	0.5706639
Decoupled trends - No trend	0.3393585	0.0329108	196	10.311453	0.0000000

Table B-6. ANOVA table comparing binomial generalized linear models of the form *ISD turnover = syndrome* and *ISD turnover = 1*.

Resid. Df	Resid. Dev	Df	Deviance	$Pr(>Chi)$
196	4.053082	NA	NA	NA
198	4.253015	-2	-0.1999328	0.9048678

Table B-7. ANOVA table comparing binomial generalized linear models of the form *Bray-Curtis dissimilarity = syndrome* and *Bray-Curtis dissimilarity = 1*.

Resid. Df	Resid. Dev	Df	Deviance	$Pr(>Chi)$
196	4.455349	NA	NA	NA
198	5.044039	-2	-0.5886892	0.7450197

B.2 Statistical comparisons of distributions in Figure 3-4

Table B-8. ANOVA table comparing ordinary linear models of the form *absolute log ratio = syndrome* and *absolute log ratio = 1*. The fit incorporating syndrome is superior to the intercept-only model ($p < 0.0001$).

Res.Df	RSS	Df	Sum of Sq	F	$Pr(>F)$
736	20.81159	NA	NA	NA	NA
738	35.42466	-2	-14.61307	258.395	0

Table B-9. Estimates (calculated using *emmeans* [63]) for the mean absolute log ratio of mean mass for routes whose dynamics for biomass were best-described by different syndromes of change. Routes with decoupled long-term trends between biomass and individuals-driven dynamics have higher absolute log ratios (mean .56, 95% credible interval .53-.58) than routes with covarying trends in biomass and individual abundance (mean of .2; 95% interval .18-.22) or no detectable temporal trend (mean of .22; .2-.24).

categorical fit	emmean	SE	df	lower.CL	upper.CL
Coupled trend	0.2007265	0.0089755	736	0.1831058	0.2183472
Decoupled trends	0.5587675	0.0137759	736	0.5317228	0.5858123
No trend	0.2211238	0.0108771	736	0.1997699	0.2424777

Table B-10. Contrasts for absolute log ratio of mean mass, calculated using *emmeans* [63].There is a significant contrast between routes with decoupled trends and the other two syndromes of dynamics (both contrasts, $p < 0.001$), but not between routes showing the "no trend" and "coupled trend" syndromes (contrast $p = .31$).

contrast	estimate	SE	df	t.ratio	p.value
Coupled trend - Decoupled trends	-0.3580410	0.0164419	736	-21.776134	0.0000000
Coupled trend - No trend	-0.0203973	0.0141022	736	-1.446391	0.3176979
Decoupled trends - No trend	0.3376437	0.0175524	736	19.236285	0.0000000

Table B-11. ANOVA table comparing binomial generalized linear models of the form *ISD turnover = syndrome* and *ISD turnover = 1*. The model incorporating syndrome is not superior to the intercept-only model ($p = .9$).

Resid. Df	Resid. Dev	Df	Deviance	$Pr(>Chi)$
736	14.09312	NA	NA	NA
738	14.28236	-2	-0.1892428	0.9097173

Table B-12. ANOVA table comparing binomial generalized linear models of the form *Bray-Curtis dissimilarity = syndrome* and *Bray-Curtis dissimilarity = 1*. The model incorporating syndrome is not superior to the intercept-only model ($p = .37$).

Resid. Df	Resid. Dev	Df	Deviance	$Pr(>Chi)$
736	20.10447	NA	NA	NA
738	22.11983	-2	-2.015363	0.3650643

REFERENCES

[1] Elita Baldridge, *MiscAbundanceDB_main*, April 2015.

[2] Elita Baldridge, David J. Harris, Xiao Xiao, and Ethan P. White, *An extensive comparison of species-abundance distribution models*, PeerJ **4** (2016), e2823.

[3] Santiago Beguería and Sergio M. Vicente-Serrano, *SPEI: Calculation of the Standardised Precipitation-Evapotranspiration Index*, 2017.

[4] Ellen K. Bledsoe and S. K. Morgan Ernest, *Temporal changes in species composition affect a ubiquitous species' use of habitat patches*, Ecology **100** (2019), no. 11, e02869.

[5] Benjamin Blonder, Lindsey Sloat, Brian J. Enquist, and Brian McGill, *Separating Macroecological Pattern and Process: Comparing Ecological, Economic, and Geological Systems*, PLOS ONE **9** (2014), no. 11, e112850.

[6] Scott A. Bonar, Jeffrey S. Fehmi, and Norman Mercado-Silva, *An overview of sampling issues in species diversity and abundance surveys*, Biological Diversity: Frontiers in Measurement and Assessment (Anne E. Magurran and Brian J. McGill, eds.), Oxford University Press, Oxford, UNITED KINGDOM, 2011, pp. 11–24.

[7] J. H. Brown, T. J. Valone, and C. G. Curtin, *Reorganization of an arid ecosystem in response to recent climate change*, Proceedings of the National Academy of Sciences **94** (1997), no. 18, 9729–9733.

[8] James H. Brown, *Organisms and Species as Complex Adaptive Systems: Linking the Biology of Populations with the Physics of Ecosystems*, Linking Species & Ecosystems (Clive G. Jones and John H. Lawton, eds.), Springer US, Boston, MA, 1995, pp. 16–24.

[9] James H. Brown, Vijay K. Gupta, Bai-Lian Li, Bruce T. Milne, Carla Restrepo, and Geoffrey B. West, *The Fractal Nature of Nature: Power Laws, Ecological Complexity and Biodiversity*, Philosophical Transactions: Biological Sciences **357** (2002), no. 1421, 619–626.

[10] James H. Brown and Brian A. Maurer, *Macroecology: The Division of Food and Space Among Species on Continents*, Science **243** (1989), no. 4895, 1145–1150.

[11] Pablo A. Cárdenas, Erica Christensen, S. K. Morgan Ernest, David C. Lightfoot, Robert L. Schooley, Paul Stapp, and Jennifer A. Rudgers, *Declines in rodent abundance and diversity track regional climate variability in North American drylands*, Global Change Biology **27** (2021), no. 17, 4005–4023.

[12] Peter Chesson, *Mechanisms of Maintenance of Species Diversity*, Annual Review of Ecology and Systematics **31** (2000), no. 1, 343–366.

[13] Chun-Huo Chiu, Yi-Ting Wang, Bruno A. Walther, and Anne Chao, *An improved nonparametric lower bound of species richness via a modified good-turing frequency formula*, Biometrics **70** (2014), no. 3, 671–682.

[14] Erica M. Christensen, David J. Harris, and S. K. Morgan Ernest, *Long-term community change through multiple rapid transitions in a desert rodent community*, Ecology **99** (2018), no. 7, 1523–1529.

[15] Erica M. Christensen, Glenda M. Yenni, Hao Ye, Juniper L. Simonis, Ellen K. Bledsoe, Renata M. Diaz, Shawn D. Taylor, Ethan P. White, and S. K. Morgan Ernest, *Portalr: An R package for summarizing and using the Portal Project Data*, Journal of Open Source Software **4** (2019), no. 33, 1098.

[16] Sean R. Connolly, Terry P. Hughes, David R. Bellwood, and Ronald H. Karlson, *Community Structure of Corals and Reef Fishes at Multiple Scales*, Science **309** (2005), no. 5739, 1363–1365.

[17] Sarah Cusser, Christie Bahlai, Scott M. Swinton, G. Philip Robertson, and Nick M. Haddad, *Long-term research avoids spurious and misleading trends in sustainability attributes of no-till*, Global Change Biology **26** (2020), no. 6, 3715–3725.

[18] Roderick C. Dewar and Annabel Porté, *Statistical mechanics unifies different ecological patterns*, Journal of Theoretical Biology **251** (2008), no. 3, 389–403.

[19] Renata M. Diaz and S. K. Morgan Ernest, *Maintenance of community function through compensation breaks down over time in a desert rodent community*, Preprint, bioRxiv, October 2021.

[20] Renata M. Diaz, Hao Ye, and S. K. Morgan Ernest, *Empirical abundance distributions are more uneven than expected given their statistical baseline*, Ecology Letters **24** (2021), no. 9, 2025–2039.

[21] Rodolfo Dirzo, Hillary S. Young, Mauro Galetti, Gerardo Ceballos, Nick J. B. Isaac, and Ben Collen, *Defaunation in the Anthropocene*, Science **345** (2014), no. 6195, 401–406.

[22] M. Dornelas, N. J. Gotelli, B. McGill, H. Shimadzu, F. Moyes, C. Sievers, and A. E. Magurran, *Assemblage Time Series Reveal Biodiversity Change but Not Systematic Loss*, Science **344** (2014), no. 6181, 296–299.

[23] Maria Dornelas, Dawn A. T. Phillip, and Anne E. Magurran, *Abundance and dominance become less predictable as species richness decreases*, Global Ecology and Biogeography **20** (2011), no. 6, 832–841.

[24] John B. Dunning, *CRC handbook of avian body masses*, 2nd ed. ed., CRC Press, Boca Raton, 2008.

[25] S. K. Morgan Ernest, *Body size, energy use, and community structure of small mammals*, Ecology **86** (2005), no. 6, 1407–1413.

[26] S. K. Morgan Ernest and James H. Brown, *Delayed Compensation for Missing Keystone Species by Colonization*, Science **292** (2001), no. 5514, 101–104.

[27] S. K. Morgan Ernest, James H. Brown, Katherine M. Thibault, Ethan P. White, and Jacob R. Goheen, *Zero Sum, the Niche, and Metacommunities: Long-Term Dynamics of Community Assembly*, The American Naturalist **172** (2008), no. 6, E257–E269.

[28] S. K. Morgan Ernest, Ethan P. White, and James H. Brown, *Changes in a tropical forest support metabolic zero-sum dynamics*, Ecology Letters **12** (2009), no. 6, 507–515.

[29] S. K. Morgan Ernest, Glenda M. Yenni, Ginger Allington, Ellen K. Bledsoe, Erica M. Christensen, Renata M. Diaz, Keith Geluso, Jacob R. Goheen, Qinfeng Guo, Edward Heske, Douglas Kelt, Joan M. Meiners, Jim Munger, Carla Restrepo, Douglas A. Samson, Michele R. Schutzenhofer, Marian Skupski, Sarah R. Supp, Kate Thibault, Shawn Taylor, Ethan White, Hao Ye, Diane W. Davidson, James H. Brown, and Thomas J. Valone, *The Portal Project: A long-term study of a Chihuahuan desert ecosystem*, bioRxiv (2020), 332783.

[30] Leonhard Euler, *Sex litterae ad Nicolaum Bernoullium II, Basileensem J. U. D. datae 1742 ad 1745*, Opera Postuma (1862), 519–549.

[31] Marco Favretti, *Remarks on the Maximum Entropy Principle with Application to the Maximum Entropy Theory of Ecology*, Entropy **20** (2018), no. 1, 11.

[32] Ingo Fetzer, Karin Johst, Robert Schäwe, Thomas Banitz, Hauke Harms, and Antonis Chatzinotas, *The extent of functional redundancy changes as species' roles shift in different environments*, Proceedings of the National Academy of Sciences **112** (2015), no. 48, 14888–14893.

[33] Jonathan A. D. Fisher, Kenneth T. Frank, and William C. Leggett, *Dynamic macroecology on ecological time-scales*, Global Ecology and Biogeography **19** (2010), no. 1, 1–15.

[34] R. A. Fisher, A. Steven Corbet, and C. B. Williams, *The Relation Between the Number of Species and the Number of Individuals in a Random Sample of an Animal Population*, Journal of Animal Ecology **12** (1943), no. 1, 42–58.

[35] S. A. Frank, *The common patterns of nature*, Journal of Evolutionary Biology **22** (2009), no. 8, 1563–1585.

[36] Steven A. Frank, *The common patterns of abundance: The log series and Zipf's law*, F1000Research **8** (2019), 334.

[37] Trevor S. Fristoe, *Energy use by migrants and residents in North American breeding bird communities*, Global Ecology and Biogeography **24** (2015), no. 4, 406–415.

[38] Janet L. Gardner, Anne Peters, Michael R. Kearney, Leo Joseph, and Robert Heinsohn, *Declining body size: A third universal response to warming?*, Trends in Ecology & Evolution **26** (2011), no. 6, 285–291.

[39] Kevin J Gaston and Tim M Blackburn, *Pattern and Process in Macroecology*, Blackwell Science Ltd, 2000.

[40] Gaston, Kevin J, Blackburn, Tim M, and Lawton, John H, *Comparing Animals and Automobiles: A Vehicle for Understanding Body Size and Abundance Relationships in Species Assemblages?*, Oikos **66** (1993), no. 1, 172–179.

[41] Andrew Gonzalez and Michel Loreau, *The Causes and Consequences of Compensatory Dynamics in Ecological Communities*, Annual Review of Ecology, Evolution, and Systematics **40** (2009), no. 1, 393–414.

[42] Nicholas J Gotelli and Robert K Colwell, *Estimating species richness*, Biological Diversity: Frontiers in Measurement and Assessment (Anne E. Magurran and Brian J. McGill, eds.), Oxford University Press, Oxford, UNITED KINGDOM, 2011, pp. 39–54.

[43] Bart Haegeman and Michel Loreau, *Limitations of entropy maximization in ecology*, Oikos **117** (2008), no. 11, 1700–1710.

[44] David J. Harris, Shawn D. Taylor, and Ethan P. White, *Forecasting biodiversity in breeding birds using best practices*, PeerJ **6** (2018), e4278.

[45] J. Harte, T. Zillio, E. Conlisk, and A. B. Smith, *Maximum Entropy and the State-Variable Approach to Macroecology*, Ecology **89** (2008), no. 10, 2700–2711.

[46] John Harte, *Maximum Entropy and Ecology: A Theory of Abundance, Distribution, and Energetics*, Oxford University Press, June 2011.

[47] John Harte and Erica A. Newman, *Maximum information entropy: A foundation for ecological theory*, Trends in Ecology & Evolution **29** (2014), no. 7, 384–389.

[48] Peter A. Henderson and Anne E. Magurran, *Linking species abundance distributions in numerical abundance and biomass through simple assumptions about community structure*, Proceedings of the Royal Society B: Biological Sciences **277** (2010), no. 1687, 1561–1570.

[49] Lucina Hernández, John W. Laundré, Alberto González-Romero, Jorge López-Portillo, and Karina M. Grajales, *Tale of two metrics: Density and biomass in a desert rodent community*, Journal of Mammalogy **92** (2011), no. 4, 840–851.

[50] C. S. Holling, *Cross-Scale Morphology, Geometry, and Dynamics of Ecosystems*, Ecological Monographs **62** (1992), no. 4, 447–502.

[51] J. E. Houlahan, D. J. Currie, K. Cottenie, G. S. Cumming, S. K. M. Ernest, C. S. Findlay, S. D. Fuhlendorf, R. D. Stevens, T. J. Willis, I. P. Woiwod, and S. M. Wondzell, *Compensatory dynamics are rare in natural ecological communities.*, Proceedings of the National Academy of Sciences. 104(9): 3273-3277 (2007).

[52] Stephen P. Hubbell, *The Unified Neutral Theory of Biodiversity and Biogeography (MPB-32)*, Princeton University Press, 2001.

[53] Brent B. Hughes, Rodrigo Beas-Luna, Allison K. Barner, Kimberly Brewitt, Daniel R. Brumbaugh, Elizabeth B. Cerny-Chipman, Sarah L. Close, Kyle E. Coblentz, Kristin L. de Nesnera, Sarah T. Drobnitch, Jared D. Figurski, Becky Focht, Maya Friedman, Jan Freiwald, Kristen K. Heady, Walter N. Heady, Annaliese Hettinger, Angela Johnson, Kendra A. Karr, Brenna Mahoney, Monica M. Moritsch, Ann-Marie K. Osterback, Jessica Reimer, Jonathan Robinson, Tully Rohrer, Jeremy M. Rose, Megan Sabal, Leah M. Segui, Chenchen Shen, Jenna Sullivan, Rachel Zuercher, Peter T. Raimondi, Bruce A. Menge,

Kirsten Grorud-Colvert, Mark Novak, and Mark H. Carr, *Long-Term Studies Contribute Disproportionately to Ecology and Policy*, BioScience **67** (2017), no. 3, 271–281.

[54] Forest Isbell, Vincent Calcagno, Andy Hector, John Connolly, W. Stanley Harpole, Peter B. Reich, Michael Scherer-Lorenzen, Bernhard Schmid, David Tilman, Jasper van Ruijven, Alexandra Weigelt, Brian J. Wilsey, Erika S. Zavaleta, and Michel Loreau, *High plant diversity is needed to maintain ecosystem services*, Nature **477** (2011), no. 7363, 199–202.

[55] E. T. Jaynes, *Information Theory and Statistical Mechanics*, Physical Review **106** (1957), no. 4, 620–630.

[56] Petr Keil, A. a. M. MacDonald, Kelly S. Ramirez, Joanne M. Bennett, Gabriel E. García-Peña, Benjamin Yguel, Bérenger Bourgeois, and Carsten Meyer, *Macroecological and macroevolutionary patterns emerge in the universe of GNU/Linux operating systems*, Ecography **41** (2018), no. 11, 1788–1800.

[57] Douglas A. Kelt, *Comparative ecology of desert small mammals: A selective review of the past 30 years*, Journal of Mammalogy **92** (2011), no. 6, 1158–1178.

[58] Douglas A. Kelt, Jaclyn R. Aliperti, Peter L. Meserve, W. Bryan Milstead, M. Andrea Previtali, and Julio R. Gutierrez, *Energetic compensation is historically contingent and not supported for small mammals in South American or Asian deserts*, Ecology **96** (2015), no. 6, 1702–1712.

[59] S. R. Kerr and L. M. Dickie, *The Biomass Spectrum: A Predator-Prey Theory of Aquatic Production*, Columbia University Press, November 2001.

[60] John H. Lawton, *What Do Species Do in Ecosystems?*, Oikos **71** (1994), no. 3, 367–374.

[61] _____, *Are There General Laws in Ecology?*, Oikos **84** (1999), no. 2, 177.

[62] Mathew A. Leibold, Jonathan M. Chase, and S. K. Morgan Ernest, *Community assembly and the functioning of ecosystems: How metacommunity processes alter ecosystems attributes*, Ecology **98** (2017), no. 4, 909–919.

[63] Russell V. Lenth, *Emmeans: Estimated Marginal Means, aka Least-Squares Means*, 2021.

[64] Simon A. Levin, *The Problem of Pattern and Scale in Ecology: The Robert H. MacArthur Award Lecture*, Ecology **73** (1992), no. 6, 1943–1967.

[65] Kenneth J. Locey and Ethan P. White, *How species richness and total abundance constrain the distribution of abundance*, Ecology Letters **16** (2013), no. 9, 1177–1185.

[66] Michel Loreau, *Does functional redundancy exist?*, Oikos **104** (2004), no. 3, 606–611.

[67] Anne E. Magurran and Peter A. Henderson, *Explaining the excess of rare species in natural species abundance distributions*, Nature **422** (2003), no. 6933, 714–716.

[68] J.G. Masek, E.F. Vermote, N.E. Saleous, R. Wolfe, F.G. Hall, K.F. Huemmrich, Feng Gao, J. Kutler, and Teng-Kui Lim, *A Landsat surface reflectance dataset for North America, 1990-2000*, IEEE Geoscience and Remote Sensing Letters **3** (2006), no. 1, 68–72.

[69] Brian A. Maurer, *Untangling ecological complexity : The macroscopic perspective*, University of Chicago Press, 1999.

[70] Brian A. Maurer and Brian J. McGill, *Measurement of species diversity*, Biological Diversity: Frontiers in Measurement and Assessment (Anne E. Magurran and Brian J. McGill, eds.), Oxford University Press, Oxford, UNITED KINGDOM, 2011, pp. 55–61.

[71] B. McGill, *Strong and weak tests of macroecological theory*, Oikos **102** (2003), no. 3, 679–685.

[72] Brian J. McGill, *The what, how and why of doing macroecology*, Global Ecology and Biogeography **28** (2019), no. 1, 6–17.

[73] Brian J. McGill, Maria Dornelas, Nicholas J. Gotelli, and Anne E. Magurran, *Fifteen forms of biodiversity trend in the Anthropocene*, Trends in Ecology & Evolution **30** (2015), no. 2, 104–113.

[74] Brian J. McGill, Rampal S. Etienne, John S. Gray, David Alonso, Marti J. Anderson, Habtamu Kassa Benecha, Maria Dornelas, Brian J. Enquist, Jessica L. Green, Fangliang He, Allen H. Hurlbert, Anne E. Magurran, Pablo A. Marquet, Brian A. Maurer, Annette Ostling, Candan U. Soykan, Karl I. Ugland, and Ethan P. White, *Species abundance distributions: Moving beyond single prediction theories to integration within an ecological framework*, Ecology Letters **10** (2007), no. 10, 995–1015.

[75] Brian Keith McNab, *Ecological factors affect the level and scaling of avian BMR*, Comparative Biochemistry and Physiology Part A: Molecular & Integrative Physiology **152** (2009), no. 1, 22–45.

[76] David Meyer, Evgenia Dimitriadou, Kurt Hornik, Andreas Weingessel, and Friedrich Leisch, *E1071: Misc Functions of the Department of Statistics, Probability Theory Group (Formerly: E1071), TU Wien*, 2019.

[77] Hélène Morlon, Ethan P. White, Rampal S. Etienne, Jessica L. Green, Annette Ostling, David Alonso, Brian J. Enquist, Fangliang He, Allen Hurlbert, Anne E. Magurran, Brian A. Maurer, Brian J. McGill, Han Olff, David Storch, and Tommaso Zillio, *Taking species abundance distributions beyond individuals*, Ecology Letters **12** (2009), no. 6, 488–501.

[78] Kenneth A. Nagy, *Field metabolic rate and body size*, Journal of Experimental Biology **208** (2005), no. 9, 1621–1625.

[79] Sean Nee, Paul H. Harvey, Robert Mccredie May, and John Richard Krebs, *Lifting the veil on abundance patterns*, Proceedings of the Royal Society of London. Series B: Biological Sciences **243** (1991), no. 1307, 161–163.

[80] Jeffrey C. Nekola and James H. Brown, *The wealth of species: Ecological communities, complex systems and the legacy of Frank Preston*, Ecology Letters **10** (2007), no. 3, 188–196.

[81] R. B. O'hara, *Species richness estimators: How many species can dance on the head of a pin?*, Journal of Animal Ecology **74** (2005), no. 2, 375–386.

[82] Jari Oksanen, F. Guillaume Blanchet, Michael Friendly, Roeland Kindt, Pierre Legendre, Dan McGlinn, Peter R Minchin, R.B. O'Hara, Gavin L. Simpson, Peter Solymos, M. Henry H. Stevens, Eduard Szoecs, and Helene Wagner, *Vegan: Community Ecology Package*, 2020.

[83] Keith L. Pardieck, David J. Ziolkowski, Michael Lutmerding, Veronica Aponte, and Marie-Anne Hudson, *North American Breeding Bird Survey Dataset 1966 - 2018, version 2018.0*, 2019.

[84] Owen L. Petchey and Andrea Belgrano, *Body-size distributions and size-spectra: Universal indicators of ecological status?*, Biology Letters **6** (2010), no. 4, 434–437.

[85] Oliver Phillips and James Stuart Miller, *Global patterns of plant diversity: Alwyn H. Gentry's forest transect data set*, vol. 89, Missouri Botanical Press, 2002.

[86] Jose Pinheiro, Douglas Bates, Saikat DebRoy, Deepayan Sarkar, and R Core Team, *Nlme: Linear and Nonlinear Mixed Effects Models*, 2020.

[87] F. W. Preston, *The Commonness, And Rarity, of Species*, Ecology **29** (1948), no. 3, 254–283.

[88] _____, *The Canonical Distribution of Commonness and Rarity: Part I*, Ecology **43** (1962), no. 2, 185–215.

[89] _____, *The Canonical Distribution of Commonness and Rarity: Part II*, Ecology **43** (1962), no. 3, 410–432.

[90] Frank W. Preston, *Gas Laws and Wealth Laws*, The Scientific Monthly **71** (1950), no. 5, 309–311.

[91] _____, *Noncanonical Distributions of Commonness and Rarity*, Ecology **61** (1980), no. 1, 88–97.

[92] R Core Team, *R: A Language and Environment for Statistical Computing*, R Foundation for Statistical Computing, 2020.

[93] Quentin D. Read, John M. Grady, Phoebe L. Zarnetske, Sydne Record, Benjamin Baiser, Jonathan Belmaker, Mao-Ning Tuanmu, Angela Strecker, Lydia Beaudrot, and Katherine M. Thibault, *Among-species overlap in rodent body size distributions predicts species richness along a temperature gradient*, Ecography **41** (2018), no. 10, 1718–1727.

[94] Jordan S. Rosenfeld, *Functional redundancy in ecology and conservation*, Oikos **98** (2002), no. 1, 156–162.

[95] John R. Sauer, William A. Link, Jane E. Fallon, Keith L. Pardieck, and David J. Ziolkowski, *The North American Breeding Bird Survey 1966–2011: Summary Analysis and Species Accounts*, North American Fauna (2013), no. 79 (79), 1–32.

[96] Aafke M. Schipper, Jonathan Belmaker, Murilo Dantas de Miranda, Laetitia M. Navarro, Katrin Böhning-Gaese, Mark J. Costello, Maria Dornelas, Ruud Foppen, Joaquín Hortal, Mark A. J. Huijbregts, Berta Martín-López, Nathalie Pettorelli, Cibele Queiroz, Axel G. Rossberg, Luca Santini, Katja Schiffers, Zoran J. N. Steinmann, Piero Visconti, Carlo Rondinini, and Henrique M. Pereira, *Contrasting changes in the abundance and diversity of North American bird assemblages from 1971 to 2010*, Global Change Biology **22** (2016), no. 12, 3948–3959.

[97] Oswald J. Schmitz, Christopher C. Wilmers, Shawn J. Leroux, Christopher E. Doughty, Trisha B. Atwood, Mauro Galetti, Andrew B. Davies, and Scott J. Goetz, *Animals and the zoogeochemistry of the carbon cycle*, Science (2018).

[98] William Shockley, *On the Statistics of Individual Variations of Productivity in Research Laboratories*, Proceedings of the IRE **45** (1957), no. 3, 279–290.

[99] Ingrid J. Slette, Alison K. Post, Mai Awad, Trevor Even, Arianna Punzalan, Sere Williams, Melinda D. Smith, and Alan K. Knapp, *How ecologists define drought, and why we should do better*, Global Change Biology **25** (2019), no. 10, 3193–3200.

[100] Felisa A. Smith, Rosemary E. Elliott Smith, S. Kathleen Lyons, and Jonathan L. Payne, *Body size downgrading of mammals over the late Quaternary*, Science **360** (2018), no. 6386, 310–313.

[101] Sarah Supp, *Manipulated Animal Community Database*, March 2014.

[102] Rebecca C. Terry and Rebecca J. Rowe, *Energy flow and functional compensation in Great Basin small mammals under natural and anthropogenic environmental change*, Proceedings of the National Academy of Sciences **112** (2015), no. 31, 9656–9661.

[103] Katherine M. Thibault and James H. Brown, *Impact of an extreme climatic event on community assembly*, Proceedings of the National Academy of Sciences of the United States of America **105** (2008), no. 9, 3410–3415.

[104] Katherine M. Thibault, S. K. Morgan Ernest, and James H. Brown, *Redundant or complementary? Impact of a colonizing species on community structure and function*, Oikos **119** (2010), no. 11, 1719–1726.

[105] Katherine M. Thibault, Sarah R. Supp, Mikaelle Giffin, Ethan P. White, and S. K. Morgan Ernest, *Species composition and abundance of mammalian communities*, Ecology **92** (2011), no. 12, 2316–2316.

[106] Katherine M. Thibault, Ethan P. White, Allen H. Hurlbert, and S. K. Morgan Ernest, *Multimodality in the individual size distributions of bird communities*, Global Ecology and Biogeography **20** (2011), no. 1, 145–153.

[107] Werner Ulrich, Marcin Ollik, and Karl Inne Ugland, *A meta-analysis of species–abundance distributions*, Oikos **119** (2010), no. 7, 1149–1155.

[108] Leigh Van Valen, *A new evolutionary law*, Evolutionary Theory **1** (1973), no. 1, 1–30.

[109] Eric Vermote, Chris Justice, Martin Claverie, and Belen Franch, *Preliminary analysis of the performance of the Landsat 8/OLI land surface reflectance product*, Remote Sensing of Environment **Volume 185** (2016), no. Iss 2, 46–56.

[110] Brian Walker, *Conserving Biological Diversity through Ecosystem Resilience*, Conservation Biology **9** (1995), no. 4, 747–752.

[111] Brian H. Walker, *Biodiversity and Ecological Redundancy*, Conservation Biology **6** (1992), no. 1, 18–23.

[112] R. M. Warwick and K. R. Clarke, *Relearning the ABC: Taxonomic changes and abundance/biomass relationships in disturbed benthic communities*, Marine Biology **118** (1994), no. 4, 739–744.

[113] Ethan P. White, *Two-phase species–time relationships in North American land birds*, Ecology Letters **7** (2004), no. 4, 329–336.

[114] Ethan P. White, S. K. Morgan Ernest, and Katherine M. Thibault, *Trade-offs in Community Properties through Time in a Desert Rodent Community.*, The American Naturalist **164** (2004), no. 5, 670–676.

[115] Ethan P. White, S.K. Morgan Ernest, Andrew J. Kerkhoff, and Brian J. Enquist, *Relationships between body size and abundance in ecology*, Trends in Ecology & Evolution **22** (2007), no. 6, 323–330.

[116] Ethan P. White, Katherine M. Thibault, and Xiao Xiao, *Characterizing species abundance distributions across taxa and ecosystems using a simple maximum entropy model*, Ecology **93** (2012), no. 8, 1772–1778.

[117] John W. Williams and Stephen T. Jackson, *Novel climates, no-analog communities, and ecological surprises*, Frontiers in Ecology and the Environment **5** (2007), no. 9, 475–482.

[118] Sharon W. Woudenberg, Barbara L. Conkling, Barbara M. O'Connell, Elizabeth B. LaPoint, Jeffery A. Turner, and Karen L. Waddell, *The Forest Inventory and Analysis Database: Database description and users manual version 4.0 for Phase 2*, Gen. Tech. Rep. RMRS-GTR-245. Fort Collins, CO: U.S. Department of Agriculture, Forest Service, Rocky Mountain Research Station. 336 p. **245** (2010).

[119] Xiao Xiao, James P. O'Dwyer, and Ethan P. White, *Comparing process-based and constraint-based approaches for modeling macroecological patterns*, Ecology **97** (2016), no. 5, 1228–1238.

[120] Hao Ye, Ellen K. Bledsoe, Renata Diaz, S. K. Morgan Ernest, Juniper L. Simonis, Ethan P. White, and Glenda M. Yenni, *Macroecological Analyses of Time Series Structure*, Zenodo, May 2020.

[121] Jian D. L. Yen, James R. Thomson, Jonathan M. Keith, David M. Paganin, Erica Fleishman, David S. Dobkin, Joanne M. Bennett, and Ralph Mac Nally, *Balancing generality and specificity in ecological gradient analysis with species abundance distributions and individual size distributions: Community distributions along environmental gradients*, Global Ecology and Biogeography **26** (2017), no. 3, 318–332.

[122] Glenda Yenni, Peter B. Adler, and S. K. Morgan Ernest, *Strong self-limitation promotes the persistence of rare species*, Ecology **93** (2012), no. 3, 456–461.

[123] Hillary S. Young, Douglas J. McCauley, Mauro Galetti, and Rodolfo Dirzo, *Patterns, Causes, and Consequences of Anthropocene Defaunation*, Annual Review of Ecology, Evolution, and Systematics **47** (2016), no. 1, 333–358.

BIOGRAPHICAL SKETCH

Renata Diaz grew up surrounded by the fields of eastern Colorado and the forests of New England, in a family of enthusiastic puzzle solvers and natural historians. During her undergraduate work in Ecology and Evolutionary Biology at Princeton University, she developed a keen interest in the interplay between theoretical, computational, and empirical modalities in ecology. For her senior thesis, she combined field experiments with a mathematical model to predict how the joint effects of large mammalian herbivores, small mammalian seed predators, and historical legacies of human-wildlife interactions modulate the spatial distribution of trees in East African savannas. From 2015 to 2017, she continued to explore dimensions of ecology as a research assistant in the Staver Lab at Yale University (2015-2016), a field intern with the Ecology of Bird Loss Project (2016), and a spatial data analysis intern in the Global Change Ecology lab at the Missouri Botanic Garden (2017). In 2017, she joined the Ernest and weecology labs at the University of Florida to pursue a PhD in macroecology, combining field work associated with The Portal Project with data- and computationally- intensive synthesis, software development projects, and intellectually adventurous theoretical pursuits.